

# **CHAPTER 4**

## **METABOLITE PROFILING AND THERAPEUTIC POTENTIAL OF MACRO-FUNGI**

**Part of this chapter has been published as:**

**Patel, R. S.**, Vanzara, A. G., Patel, N. R., Vasava, A. M., Patil, S. M., and Rajput, K. S. (2020). In-silico discovery of fungal metabolites bergenin, quercitrin and dihydroartemisinin as potential inhibitors against main protease of SARS-CoV-2. *Coronaviruses*, 1, 1-23.

**4.1. Introduction**

Fungi are biotechnologically important yet understudied group of microorganisms. They have developed several survival mechanisms as a result of their wide diversity of habitats and the necessity to compete against a broad array of organisms. The urge for the studies on biodiversity of fungi and the establishment of fungal collection, have enormous economic potential in terms of identifying organisms with distinct commercial applications that will produce novel products (Hyde et al., 2019). Nowadays, there is an increased attention in fungi not just as a high protein food but also as a resource of biologically active compounds having therapeutic potential like anticancer, immunopotentiating, hepatoprotective, antiviral etc (Rathee et al., 2012). In order to discover the innovative therapeutic possibilities, more research is required into the mechanisms underlying the multiple health benefits of the fungus to humans.

The screening of the secondary metabolite is almost entirely motivated by the discovery for novel bioactive compound in therapeutics since many years. It is because of fungal secondary metabolites that have such a wide range of chemical structures (generally terpenoids, polyketides, non-ribosomal peptides and mixed structures), determining their analytical properties, isolating them, and deciphering their detailed structures has remained a major technical challenge (Martín et al., 2014). With the recent advancements in analytical instrumentation and computational biology, studying bioactive compounds from fungi and screening of the new metabolites for medicinal purposes may become easier. Metabolite profiling is a tool that may be used to find diverse applications in all aspects of understanding, utilization and discovery, making it a key point in studies of fungal physiology and taxonomy (Smedsgaard and Nielsen, 2005). In a view of this background, the study

was focused on therapeutic application of bioactive metabolites extracted from fungi and their identification by HR-LC/MS.

## **4.2. Material and Methodology**

### **4.2.1. Materials**

All the reagents and chemicals utilized in the present investigation were of analytical grade and purchased from SIGMA, Merck and SRL. Potato dextrose broth and agar were procured from HiMedia, India, MTT [3-(4, 5-dimethylthiazole-2-yl)-2, 5-diphenyl tetrazolium bromide] from SRL, India, DPPH• (2-deoxy-o-ribose and 1,1-diphenyl-2-picrylhydrazyl), dimethyl sulphoxide (DMSO) and Dulbecco's Modified Eagle's Medium (DMEM) from Sigma, USA. Ascorbic acid and hydrogen peroxide (H<sub>2</sub>O<sub>2</sub>) were procured from SRL, India.

### **4.2.2. Fungal strains**

Out of the several fungal strains screened, seven species viz. *Pisolithus albus*, *P. tinctorius*, *Geastrum triplex*, *G. saccatum*, *Dictyophora indusiata*, *Itajahya galariculata* and *Cyathus stercoreus* were used to check their therapeutic potential. The collected fruiting bodies were dried in an oven before being pulverised into a fine powder with an electric grinder. The powder was kept in airtight bags for future use.

### **4.2.3. Extraction of fungal compounds**

Powders (20g) of each of the selected seven fungi were soaked in 85% ethanol overnight at 30°C under vigorous shaking conditions (110 rpm). In order to obtain the dried residue, the ethanol phase was filtered with Whatman No. 1 filter paper and then concentrated using a rotary evaporator. The obtained residues were further dissolved in 10% DMSO and used for the metabolic profiling of bioactive metabolites and the evaluation of their therapeutic effects.

#### 4.2.4. Antioxidant assays

The ethanolic extracts of all the fungi were tested for antioxidant activity against DPPH and H<sub>2</sub>O<sub>2</sub>.

##### 4.2.4.1 DPPH scavenging potential

The radical scavenging potential of ethanolic extracts of these fungi was investigated using the method described by Blois, (1958). A solution of 0.06 mM ( $6 \times 10^{-5}$ ) DPPH was prepared in DMSO. The reaction system comprised of 1 ml of ethanolic fungal extract at a concentration varying from 50 to 200 mg/ml and 1 ml of DPPH solution. After adding the DDPH to the mixture, it was shaken immediately. Then the incubation was carried out for an hour in the dark at room temperature. The reduction in absorbance was measured using a spectrophotometer at a wavelength of 517 nm. An ascorbic acid sample was used as a positive control, a sample without DPPH solution was used as a control, and DMSO was used as a blank. The DPPH scavenging potential was calculated by employing the equation (1).

$$\text{DPPH scavenging activity \%} = \frac{(A_0 - A_1)}{A_0} \times 100 \dots \dots \dots (1)$$

Where, A<sub>0</sub> = absorbance of the control. A<sub>1</sub> = absorbance of the sample.

##### 4.2.4.2 Hydrogen peroxide scavenging potential

The H<sub>2</sub>O<sub>2</sub> scavenging potential of fungal ethanolic extracts was assessed using the methodology published by Zhao et al., (2006). As a first step, a solution of 2 mM H<sub>2</sub>O<sub>2</sub> was prepared in 100 mM sodium phosphate (pH 7.4). The reaction mixture was comprised of 1 ml of ethanolic fungal extract at varying concentrations (50-200 µg/ml) and 1 ml H<sub>2</sub>O<sub>2</sub> solution. After that, the tubes were incubated for 10 minutes under the dark condition at room temperature. A spectrophotometer was used to measure the absorbance at 230 nm. A positive control was ascorbic acid, whereas

phosphate buffer without H<sub>2</sub>O<sub>2</sub> was utilized as a blank. The scavenging potential of H<sub>2</sub>O<sub>2</sub> was calculated by employing the equation (2).

$$\text{H}_2\text{O}_2 \text{ scavenging activity (\%)} = \frac{(A_0 - A_1)}{A_0} \times 100 \dots \dots \dots (2)$$

Where, A<sub>0</sub>: absorbance of the control and A<sub>1</sub>: absorbance of the extract/standard.

#### **4.2.5. Anticancer assays**

##### **4.2.5.1. Human cancer cell lines and maintenance**

Human cancer cell lines namely human breast adenocarcinoma, MDA-MB-231; human lung cancer cells, A549 and human colorectal cancer cells, HCT116 were tested for anticancer activity. All the cell lines were procured from NCCS (National Centre for Cell Science) Pune, India and grown at 37°C with 5% CO<sub>2</sub> in DMEM.

##### **4.2.5.2. MTT assay**

Cytotoxicity of the all the fungal crude extracts against MDA-MB-231, A549 and Caco-2 cell lines was determined by MTT assay. The cell suspension was incorporated to the 96-well plates at concentrations of 1x10<sup>5</sup> cells/ml. Then the cells were treated with varying concentrations of fungal crude extracts (50-200 µg/ml) and the plates were incubated for 24 h in a incubator (humidity-controlled) containing 5% CO<sub>2</sub> at 37°C. Washing of cells was carried out using phosphate buffered saline (PBS) and then incubated for 4 h. About 100 µl of the MTT solution (5 mg/mL) was supplemented to each well and the plate was placed at 37°C for 1 h. To solubilize the crystals of formazan, the medium was first removed and then 100 µl of DMSO was incorporated. Using an ELISA reader, the quantity of formazan crystal was assessed by doing measurement of absorbance at the wavelength of 570 nm. All the experiments were run in triplicate to determine the IC<sub>50</sub> value which is the amount of crude extract required to reduce the absorbance to half that of the control. The % of

inhibition was computed by employing the equation (3) as published by Seetharaman et al., (2017).

$$\% \text{ of cytotoxicity} = \frac{\text{Absorbance of control} - \text{Absorbance of sample}}{\text{Absorbance of control}} \times 100 \dots \dots \dots (3)$$

Where, Absorbance of control is the mean optical density of untreated cells and Absorbance of sample is the mean optical density of treated cell.

#### ***4.2.6. Identification and analysis of fungal metabolites by High Resolution-Liquid Chromatography Mass Spectroscopy (HR-LC/MS)***

Using ultrahigh performance liquid chromatography coupled with a pulsed desorption cyclotron (HR-LCMS 1290 Infinity UHPLC System, Agilent Technologies®, USA), a comprehensive profile of bioactive compounds was carried out from crude extracts of selected fungi. The liquid chromatography system comprised MS Q-TOF (G6550A), two ions sources (Dual AJS ESI), a binary pump (G4220B), a HiP sampler (G4226A), and Column Comp (G1316C). The system was injected with three microlitres of samples, followed by separation on the SB-C18 column (2.1 329 × 50 mm, 1.8 micron particle size). The mobile phase used in this study was made up of 100% water (aqueous formic acid 0.1% (v/v) - solvent A) and 100% acetonitrile (90% acetonitrile + 10% water + 0.1% formic acid - solvent B). In the beginning, 95% of solvent A and 5% of solvent B were used for two minutes, followed by 100% B after 16 minutes. After maintaining this solvent composition for eight minutes (100% B), the conditions were returned to the initial conditions. The rate of flow was set to 100 µl/min. Mass spectra and mass fragmentation patterns were used to identify compounds.

#### ***4.2.7. In silico analysis of fungal metabolites as potential inhibitors against main protease of SARS-CoV-2***

##### ***4.2.7.1. Proteins/Macromolecules***

Virtual screening was initiated using the crystallographic structure of SARS-CoV-2 M<sup>pro</sup> with an inhibitor N3 (Jin et al., 2020). The structure was retrieved from Protein Data Bank (PDB) with accession number 6LU 7 (Deposited: 2020-01-26; Released: 2020-02-05). The 6LU7 protein is a homodimer with two chains, A and C. Macromolecule preparation was carried out using chain A. The native ligand for 6LU7 is N-[(5-METHYLISOXAZOL-3-YL)CARBONYL]ALANYL-L-VALYL-N~1~-((1R,2Z)-4-(BENZYL OXY)-4-OXO-1-{[(3R)-2-OXOPYRROLIDIN-3-YL]METHYL}BUT-2-ENYL)-L-LEUCINAMIDE (Khaerunnisa et al., 2020).

##### ***4.2.7.2 Ligand and drug download***

ZINC and PubChem database were used to obtain 3D structures of natural compounds obtained from the above-mentioned species. Bergenin (ZINC4046820) and quercitrin (ZINC4175638) were downloaded from (ZINC database) whereas dihydroartemisinin (CID 456410) was downloaded from PubChem in sdf format. Downloaded compounds were restricted to Lipinski's rule of five for drug-likeness properties which include no more than 10 hydrogen bond acceptors, no more than 5 hydrogen bond donors, molecular weights between 160 and 500 g/mol and logP between -0.4 and 5.6 (Lipinski et al., 1997). Drug-likeness properties with Lipinski's rule of five were calculated using SWISSADME prediction.

##### ***4.2.7.3. Determination of active sites***

The co-ordinates of N3 binding site on SARS-CoV-2 M<sup>pro</sup> were determined using UCSF Chimera (version 1.14), Biovia Discovery Studio 2020 and also according to

previous studies with the crystallographic structure of SARS-CoV-2 M<sup>pro</sup> (Andrade et al., 2020; Jin et al., 2020; Wang et al., 2020; Zhang et al., 2020). The determined amino acids (THR190, GLU166, GLN189, GLY143, HIS163, HIS164, CYS145 and PHE140) in the active site were used to analyse the grid box for evaluation of docking results.

#### ***4.2.7.4. Molecular Docking***

Ligand was first converted into pdb format from sdf format using an Open Babel GUI 3.0 software. The structures of all the ligand molecules and 6LU7 protein molecule were converted to their corresponding pdbqt files using AutoDock Tools 1.5.6 (Morris et al., 2009). Protein optimization was carried out by removing water and other atoms, adding polar hydrogen group and Kollman charges using AutoDock version 4.2.6 which is supported by AutoDock tools, MGL tools, AutoDockvina and AutoGrid. The grid coordinates (X, Y, and Z) were arranged on the active site region to define a gridbox. Each docking run was performed 4 times using genetic algorithm (GA) parameters with 1750000 generations. The docking analysis was performed by AutoDock 4.2.6. The 10 best docking hits were selected based on the average of affinity energy values. To confirm the interactions of molecule with the amino acids within the protease active site, the docking positions were analysed using PyMol 2.3 (Schrödinger, 2020). Discovery Studio Visualizer 2020 was used for generating 2D maps of receptor-ligand interactions.

#### ***4.2.7.5. ADMET study***

The predicted Absorption Distribution Metabolism, Excretion and Toxicity (ADMET) study were analyzed using the pkCSM - pharmacokinetics server (Pires et al., 2015). The sdf file of the compounds were converted into SMILES (Simplified Molecule



Input Line Entry Specification) using an Open Babel GUI 3.0 software and uploaded to pkCSM to calculate the ADMET properties using default parameters.

### **4.3. Results and discussion**

#### ***4.3.1. Collection and extraction of fungal specimens***

In determining the therapeutic potential of medicinal fungi, the first crucial step is extraction as it is so important to extract the preferred bioactive components out of the fungal fruiting bodies. The fundamental process comprised steps like pre-washing of fungal material, drying or freeze-drying, size reduction via grinding to gain a homogenous powder, extraction with a solvent system, filtration, concentration, drying, and reconstitution. Appropriate actions must be needed to ensure that potential bioactive compounds are not distorted or lost at the time of extract preparation. The selection of a proper solvent system is also most important for the separation of bioactive compounds acquired out of the fungal material, which mainly rely on the specified nature of the targeted bioactive compounds. In the present study, collected fungal fruiting bodies were dried, grounded into a fine powder, and extracted with ethanol (85%) via maceration technique for the extraction of different bioactive compounds.

#### ***4.3.2 Antioxidant potential***

##### ***4.3.2.1. DPPH scavenging potential***

The assay of DPPH• is a method for determining antioxidant activity in a shorter period of time than other procedures. Furthermore, certain side reactions such as enzyme inhibition and metal chelation have little effect on DPPH•, which is a major disadvantage of laboratory-generated free radicals (Oyetayo et al., 2009). The scavenging potentials were found to be 10.03% and 14.03% at 50 µg/ml concentration of ethanolic extracts of *P. albus* and *P. tinctorius*, respectively which were augmented

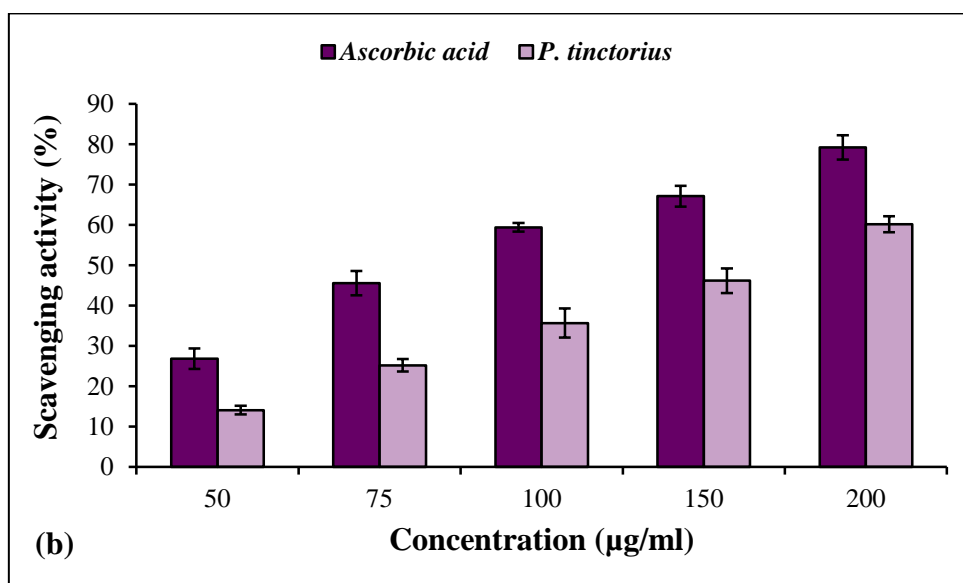
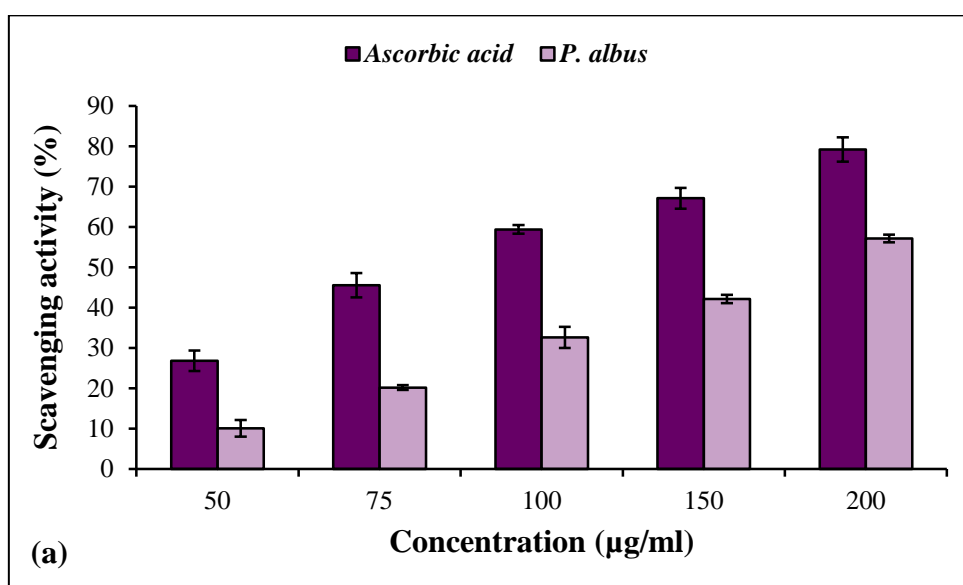
in concentration dependent mode (**Fig. 4.1a and b**). The ethanolic extracts of *P. albus* and *P. tinctorius* exhibited the scavenging potential maxima of 57.12% and 60.12%, respectively at 200 µg/ml concentration. The results clearly specified that there is no tangible distinction between the scavenging potentials of *P. albus* and *P. tinctorius*.

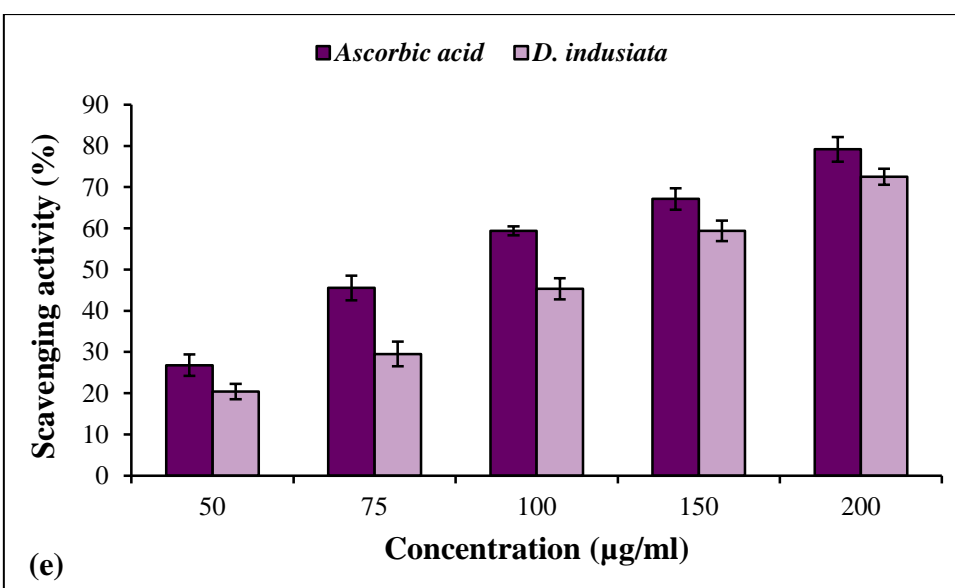
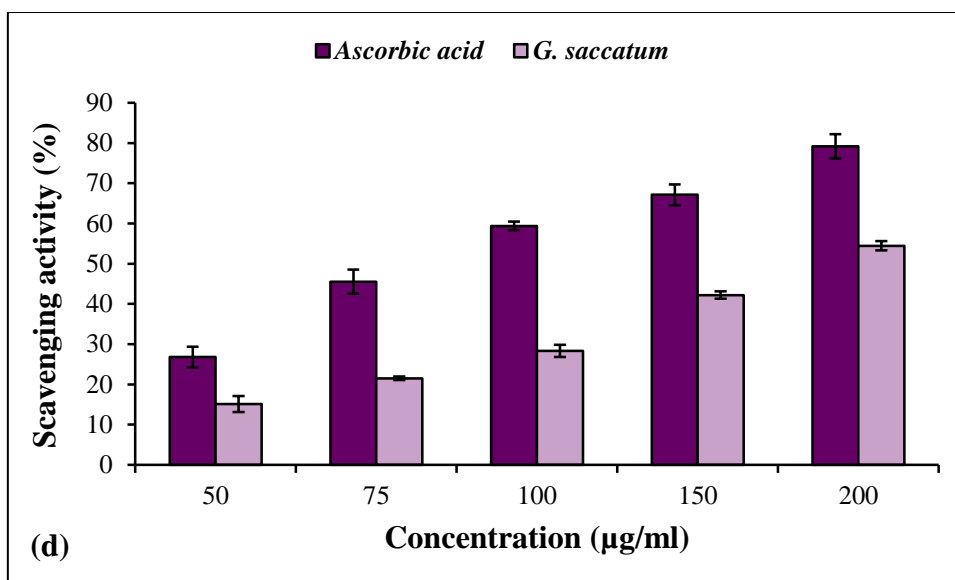
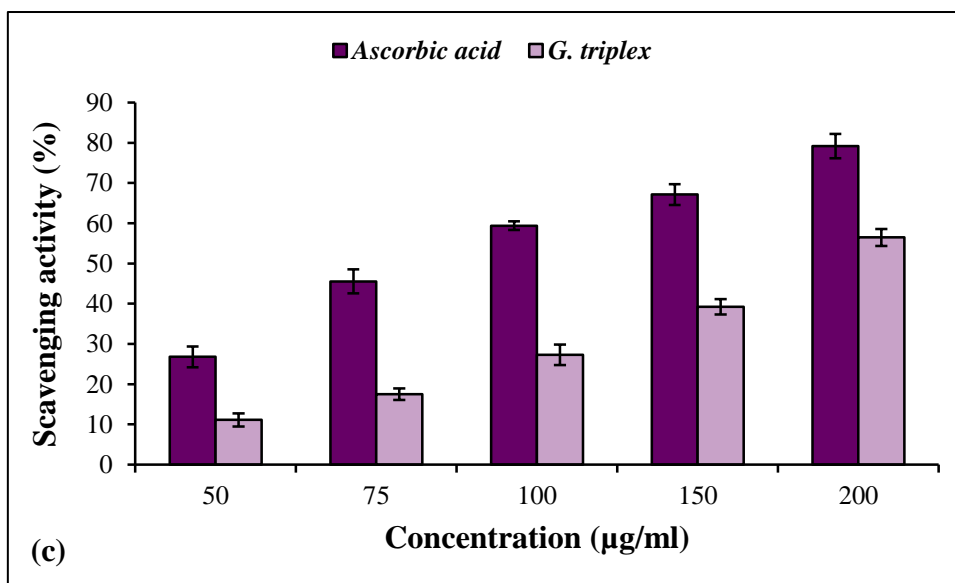
The scavenging potentials were found to be 11.12% and 15.12% at 50 µg/ml concentration of ethanolic extracts of *G. triplex* and *G. saccatum*, respectively which were augmented in concentration dependent mode (**Fig. 4.1c and d**). The ethanolic extracts of *G. triplex* and *G. saccatum* showed the maximum scavenging potential of 56.47% and 45.82%, respectively at 200 µg/ml concentration. The results clearly indicated that there is no tangible distinction between the scavenging potentials of *G. triplex* and *G. saccatum*.

The ethanolic extract of *D. indusiata* was an effective free radical scavenger (**Fig. 4.1e**). At 50-200 µg/ml concentration, the ethanolic extract exhibited 20.41 to 72.53% scavenging potential. The results clearly indicated that ethanolic extract of *D. indusiata* possess concentration dependent scavenging effect. Earlier report on the methanolic extract and water extract from *D. indusiata* showed an excellent scavenging effect of 92.1% and 97.58% on DPPH• radicals at 6400 µg/ml and 2000 µg/ml (Mau et al., 2002; O Oyetayo et al., 2009). However, in the present investigation, the ethanolic extract from *D. indusiata* exhibited maximum of 72.53% scavenging activity at inferior concentration of 200 µg/ml. These findings clearly depict that ethanolic extract of *D. indusiata* has good scavenging efficacy against DPPH• radicals.

The scavenging potential for ethanolic extract of *I. galariculata* was found to be 17.31-64.64% at 50-200 µg/ml concentration (**Fig. 4.1f**). At 50-200 µg/ml

concentration, the *C. stercoreus* extract exhibited 9.04 to 46.21% scavenging potential (Fig. 4.1g). The results clearly indicated that ethanolic extracts of *I. galericulata* and *C. stercoreus* possess concentration dependent scavenging effect. Overall, the scavenging potentials were *D. indusiata* > *I. galericulata* > *P. tinctorius* > *P. albus* > *G.triplex* > *G. saccatum* > *C. stercoreus*. Within the studied concentration range, the ability of ascorbic acid to scavenge DPPH radicals in each case was noticeably greater than those of ethanolic extract.





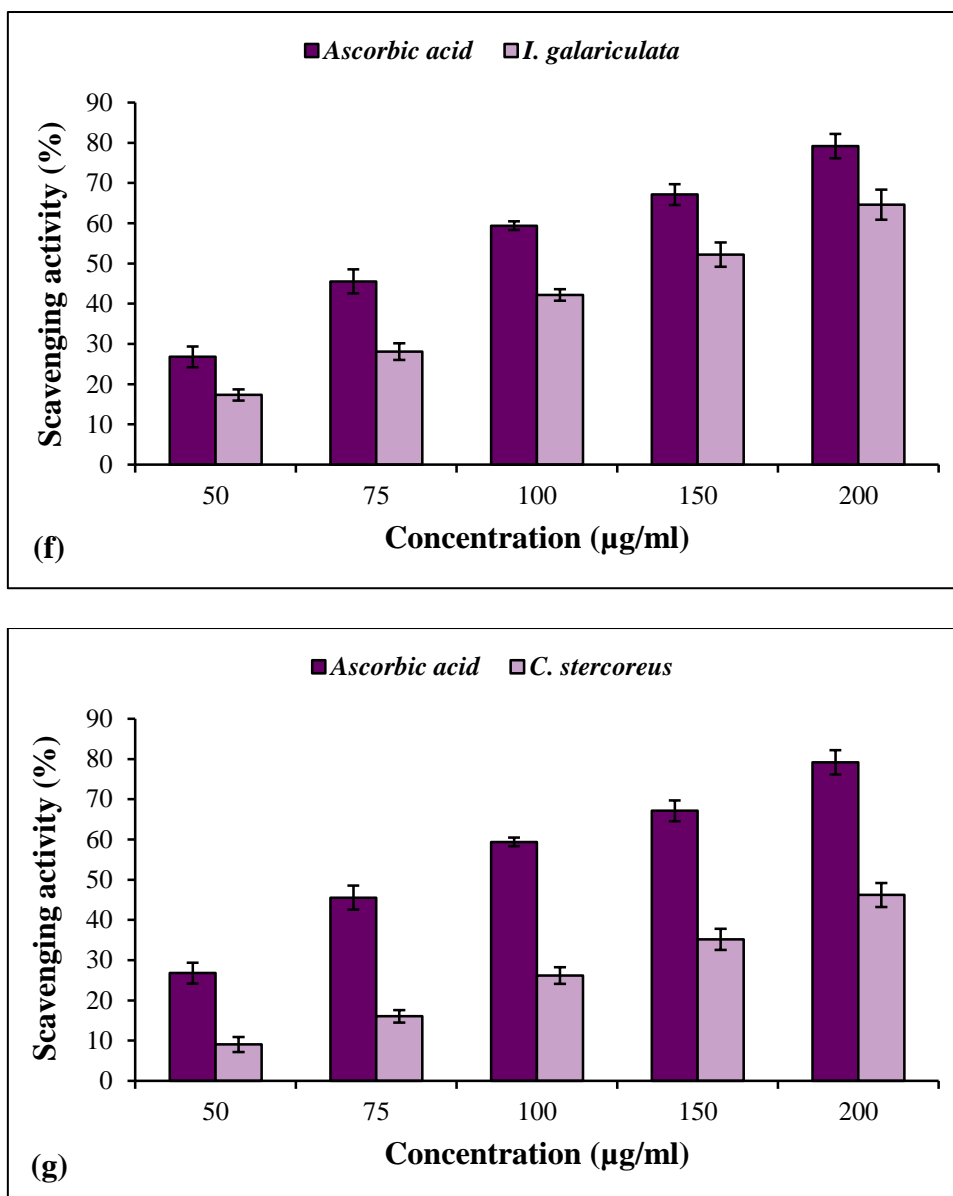


**Fig. 4.1:** Antioxidant potentials of different fungal crude extracts at different concentration against DPPH free radicals. (a) *P. albus* (b) *P. tinctorius* (c) *G. triplex* (d) *G. saccatum* (e) *D. indusiata* (f) *I. galariculata* (g) *C. stercoreus*

#### 4.3.2.2. Hydrogen peroxide scavenging potential

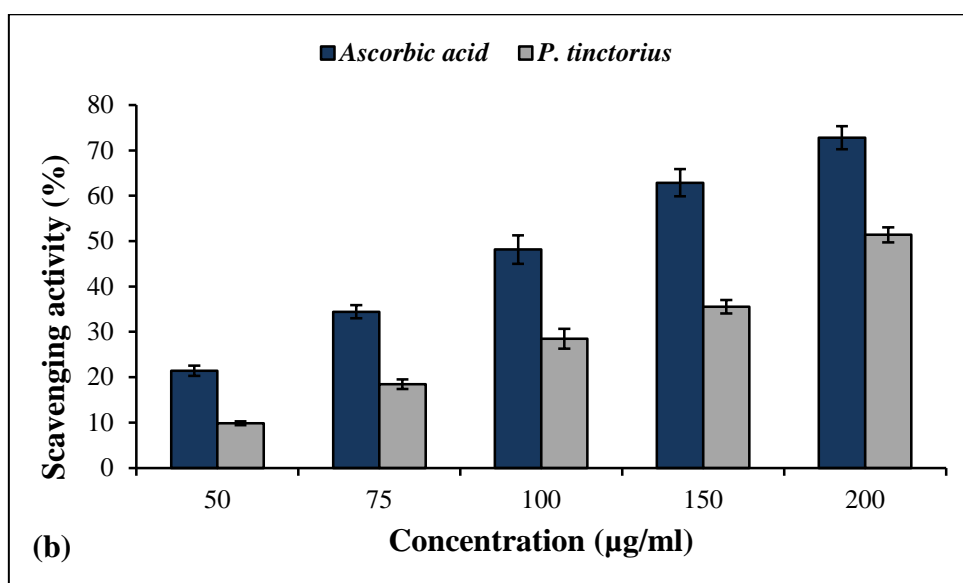
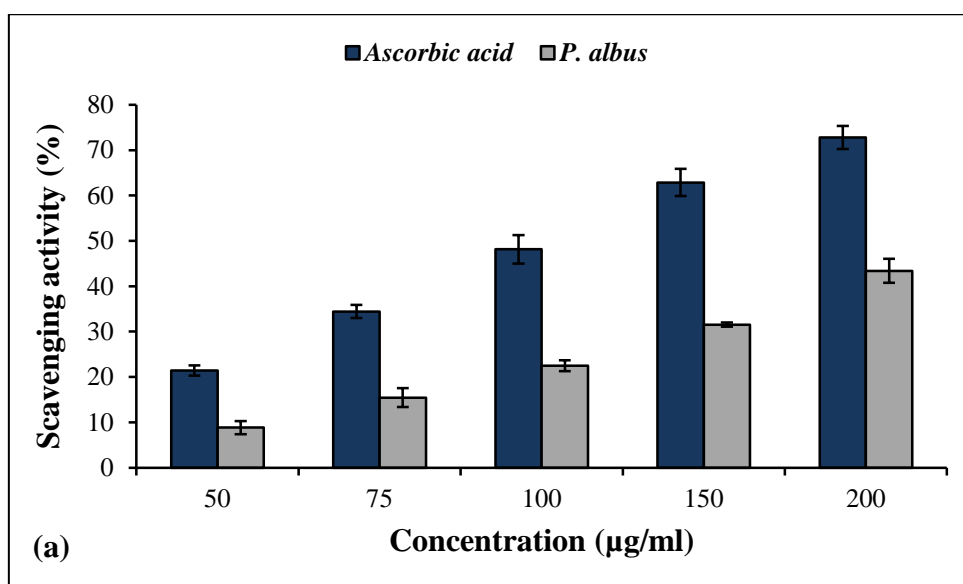
Hydroxyl radicals are produced by the iron-catalyzed Fenton or Haber-Weiss reactions, and are highly reactive which can cause oxidative damage to the biomolecules. However, antioxidants can lower the amount of hydroxyl radicals

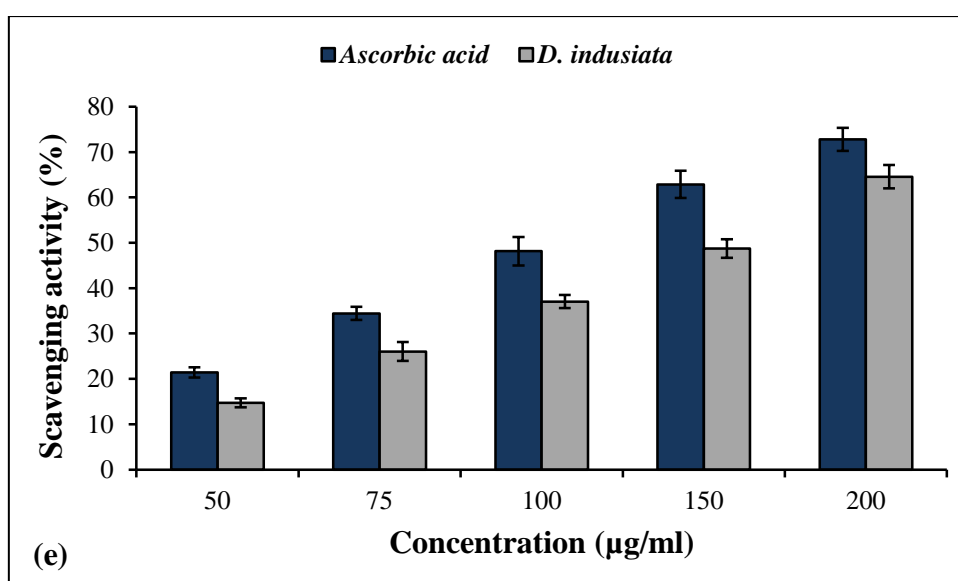
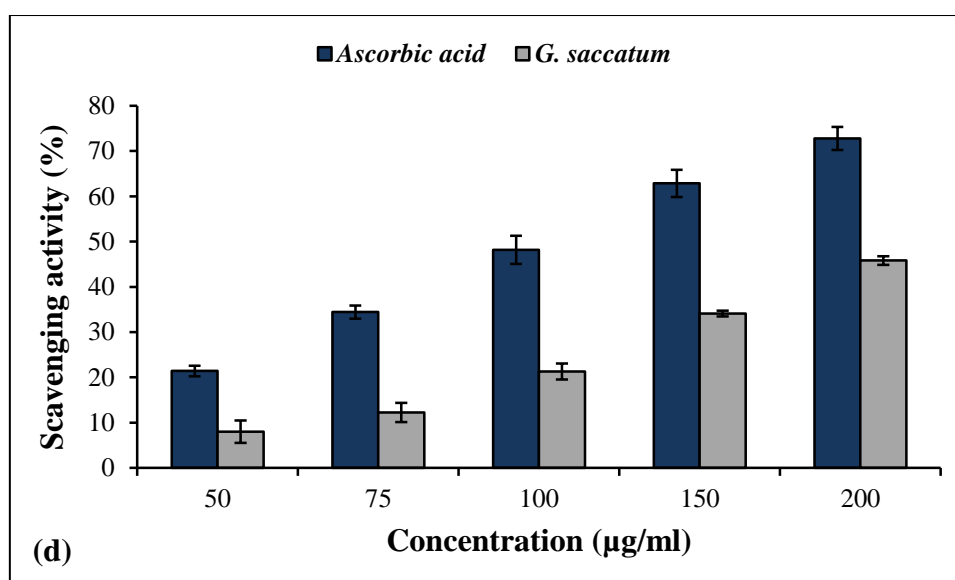
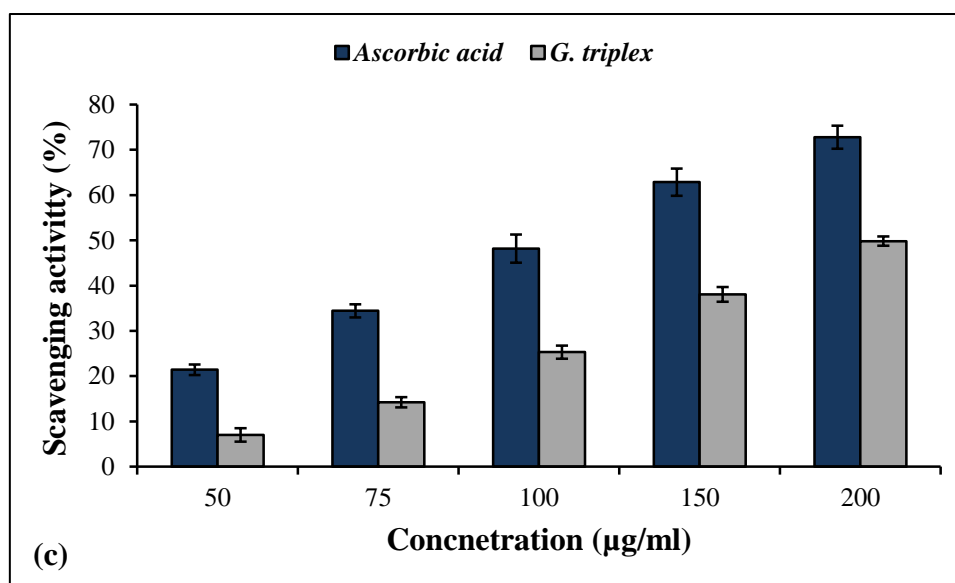
produced (Liu et al., 2017). The scavenging potentials of different fungal ethanolic extract on hydroxyl radicals are shown in **Fig. 4.2**.

The scavenging potentials were found to be 8.85% and 9.85% at 50 µg/ml concentration of ethanolic extracts of *P. albus* and *P. tinctorius*, respectively (**Fig. 4.2a** and **b**). The ethanolic extracts of *P. albus* and *P. tinctorius* exhibited the scavenging potential maxima of 57.12% and 51.39%, respectively at 200 µg/ml concentration. The results clearly indicated that there is no tangible distinction between the scavenging potentials of *P. albus* and *P. tinctorius*. The scavenging potentials were found to be 7.02% and 8.02% at 50 µg/ml concentration of ethanolic extracts of *G. triplex* and *G. saccatum*, respectively (**Fig. 4.2c** and **d**). The ethanolic extracts of *G. triplex* and *G. saccatum* showed the maximum scavenging potential of 49.82% and 45.82%, respectively at 200 µg/ml concentration. The results clearly indicated that there is no tangible distinction between the scavenging potentials of *G. triplex* and *G. saccatum*. The scavenging activity of ethanolic extract of *D. indusiata* was increased from 14.72% to 64.56% within the concentration range of 50 µg/ml to 200 µg/ml (**Fig. 4.2e**). The scavenging activity of ethanolic extract of *I. galariculata* was increased from 12.14% to 56.43% within the concentration range of 50 µg/ml to 200 µg/ml (**Fig. 4.2f**). At 50-200 µg/ml concentration, the ethanolic extract of *C. stercoreus* exhibited 6.40 to 46.90% scavenging potential (**Fig. 4.2g**).

Overall, the results clearly specified that the ethanolic extract of all the tested fungi has scavenging potential on hydroxyl radicals in a concentration-dependent manner. In each of the case, the scavenging potential of ascorbic acid on hydroxyl radicals was significantly higher than that of ethanolic extract within the tested concentration

range. Moreover, the scavenging potentials were *D. indusiata* > *I. galariculata* > *P. tinctorius* > *P. albus* > *G. triplex* > *G. saccatum* > *C. stercoreus*.







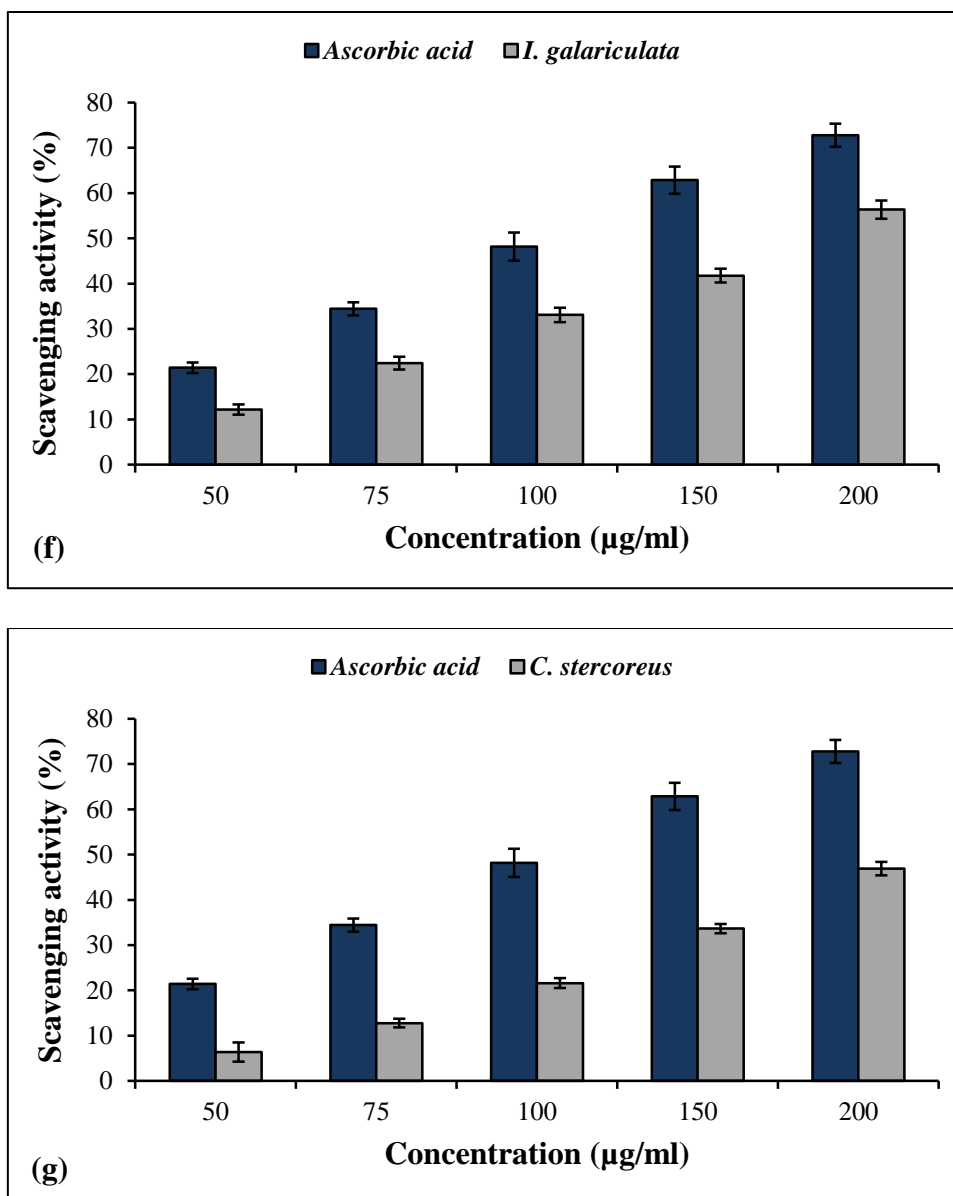


**Fig. 4.2:** Antioxidant potentials of different fungal crude extracts at different concentration against H<sub>2</sub>O<sub>2</sub>. (a) *P. albus* (b) *P. tinctorius* (c) *G. triplex* (d) *G. saccatum* (e) *D. indusiata* (f) *I. galariculata* and (g) *C. stercoreus*

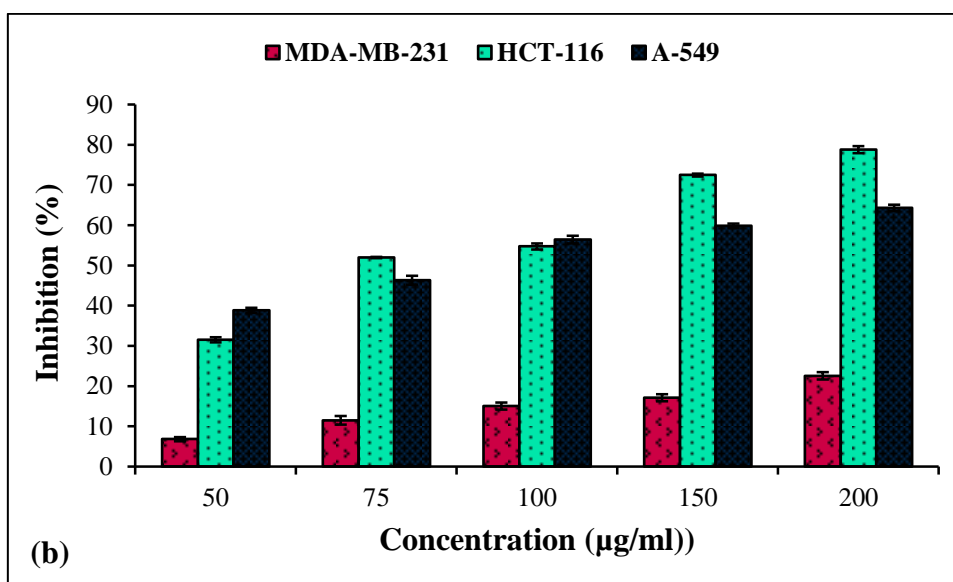
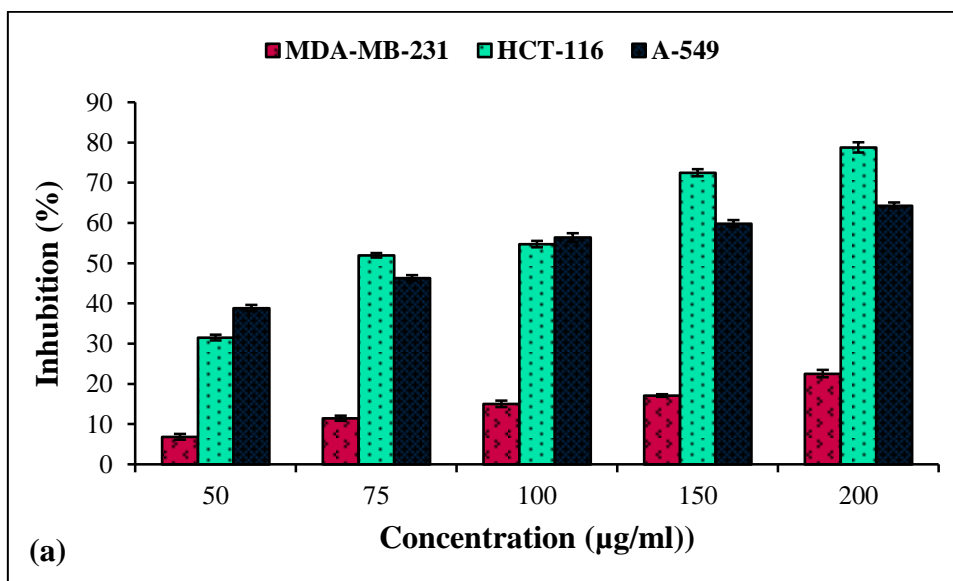
#### 4.3.3. Anticancer activity

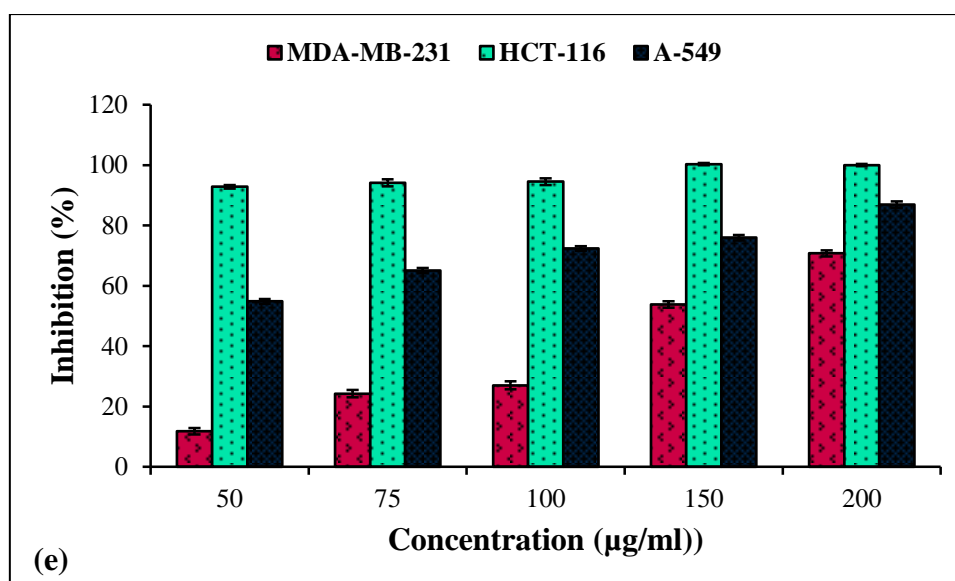
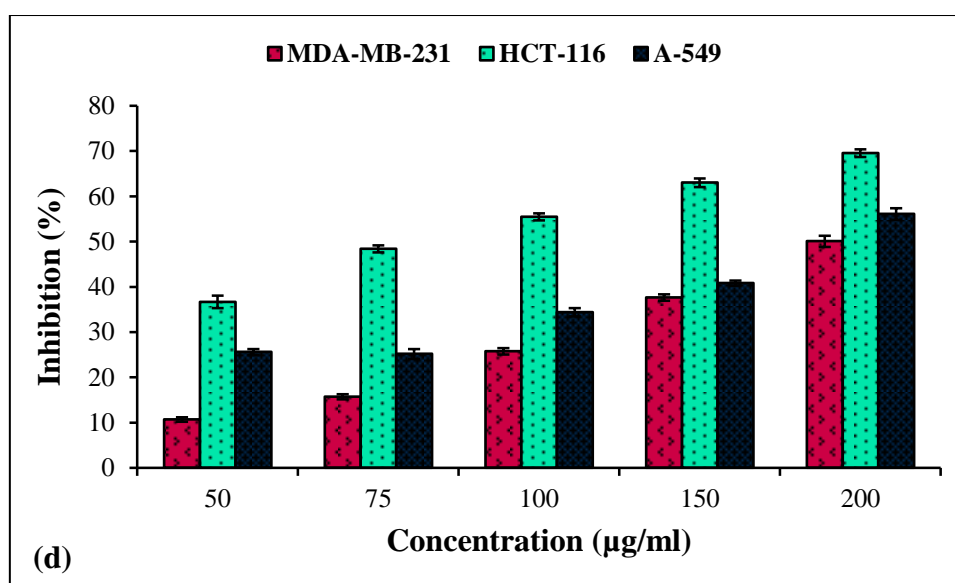
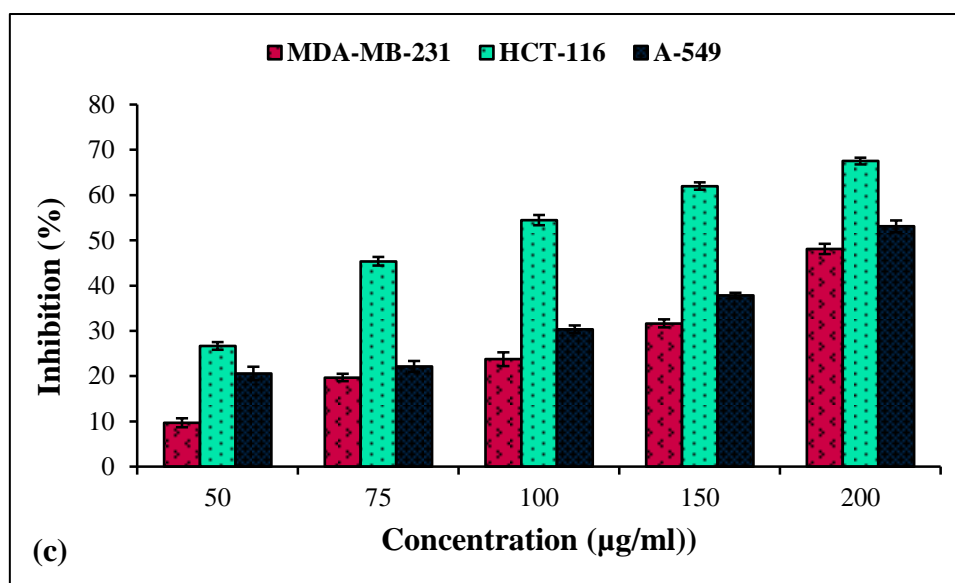
Around the globe, cancer-related deaths are increasing as the incidence continues to rise (Bray et al., 2018). As stated by the World Health Organization (WHO), colorectal cancer, breast cancer, and lung cancer are the three malignancies that are

most frequently diagnosed internationally and continue to be the primary cause of cancer-related deaths globally (Sung et al., 2021). Conventional cancer treatments are still the most common form of treatment, despite being mainly unsuccessful and causing many deaths due to the side effects. In contrast, developing new cancer treatments derived from natural sources with fewer side effects have become an exciting field of research (Zhang et al., 2018). Fungi are regarded as a potential repository of novel chemical compounds for cancer research (Iqbal et al., 2017). Many well-known anticancer compounds have been reported from different fungi (Desai et al., 2008). A biogeographically different region, provides a remarkably rich source of different medicinal fungi with anticancer properties (Evidente et al., 2014). The Gujarat state is widely renowned for having wide range of climatic conditions starting from moist deciduous (South Gujarat) to scrub forest (North Gujarat, Saurashtra, Kachh) including pure desert conditions in Rann of Kachh is therefore one of the ideal places to explore the therapeutic properties of fungi.

The anticancer potential of crude extract of seven different species of fungi that are medicinally important were evaluated against three different cancer cell lines viz MDA-MB-231, HCT-116 and A-549 by MTT assay. The data of inhibition (%) of crude extracts of seven different fungi against three cancer cell lines has been shown in **Fig. 4.3**. Significant inhibition of colorectal cancer cells HCT-116 was found then lung cancer cells A-549 and breast cancer cells MDA-MB-231. The crude extracts of *D. indusiata*, *P. albus*, *P. tinctorius*, *I. galariculata* and *C. stercoreus* had highest inhibition activity towards HCT-116 whereas *G. saccatum* and *G. triplex* had moderate inhibition activity. The crude extracts of *D. indusiata* and *I. galariculata* had highest inhibition activity towards A-549 whereas *P. albus*, *P. tinctorius*, *G. saccatum*, *G. triplex* and *C. stercoreus* had moderate inhibition activity. The crude

extract of *D. indusiata* had highest inhibition activity towards MDA-MB-231; *I. galariculata*, *G. saccatum* and *G. triplex* had moderate inhibition activity whereas *P. albus*, *P. tinctorius* and *C. stercoreus* had lowest inhibition activity. Dose-dependent anticancer potential of fungal extracts was observed i.e. increase in concentration (50, 75, 100, 150 and 200 µg/ml), escalates the potentiality of selected fungus.





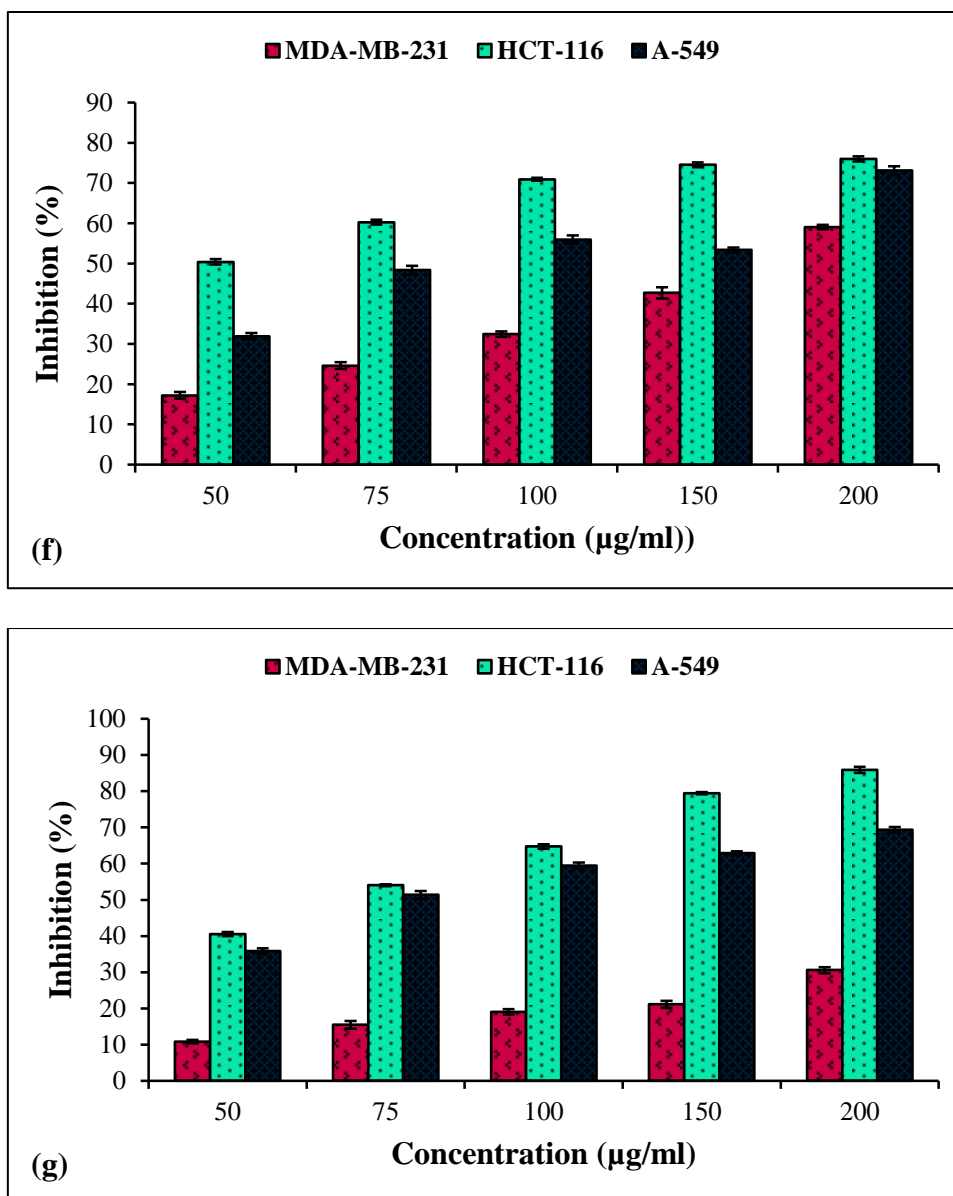


**Fig. 4.3:** Anticancer potentials of different fungal crude extracts at different concentration on various cancerous cell lines. (a) *P. albus* (b) *P. tinctorius* (c) *G. triplex* (d) *G. saccatum* (e) *D. indusiata* (f) *I. galariculata* and (g) *C. stercoreus*

#### 4.3.4. Identification and analysis of fungal metabolites by High Resolution-Liquid Chromatography Mass Spectroscopy (HR-LC/MS)

Fungi are well known for their significant bioactive potentials, including antiviral capability; therefore, crude extracts of five selected fungi were used for profiling of

their bioactive compounds using HR-LC/MS. With the detailed mass spectrum data (Fig. 4.4 to 4.8), absorbance spectra and retention times were compared with the available literature and found that all the fungi possess different bioactive compounds which belong to various classes. The identified bioactive compounds from the crude extracts of *P. albus*, *G. triplex*, *D. indusiata*, *I. galariculata* and *C. stercoreus*, and their therapeutic potential have been shown in Table 4.1 to 4.5.

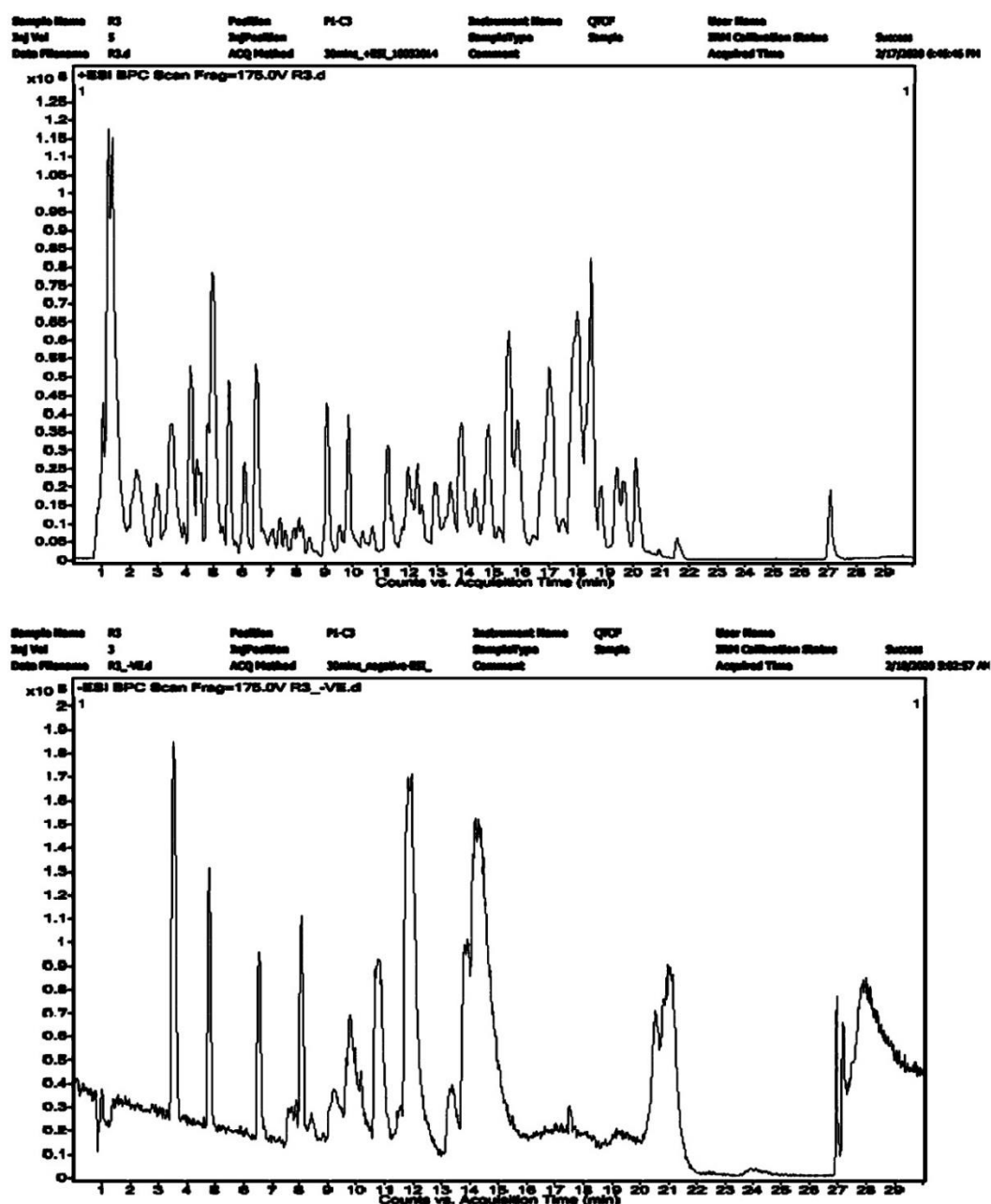


Fig. 4.4: HR-LC/MS analysis of crude extract of *P. albus* in +ve and -ve mode

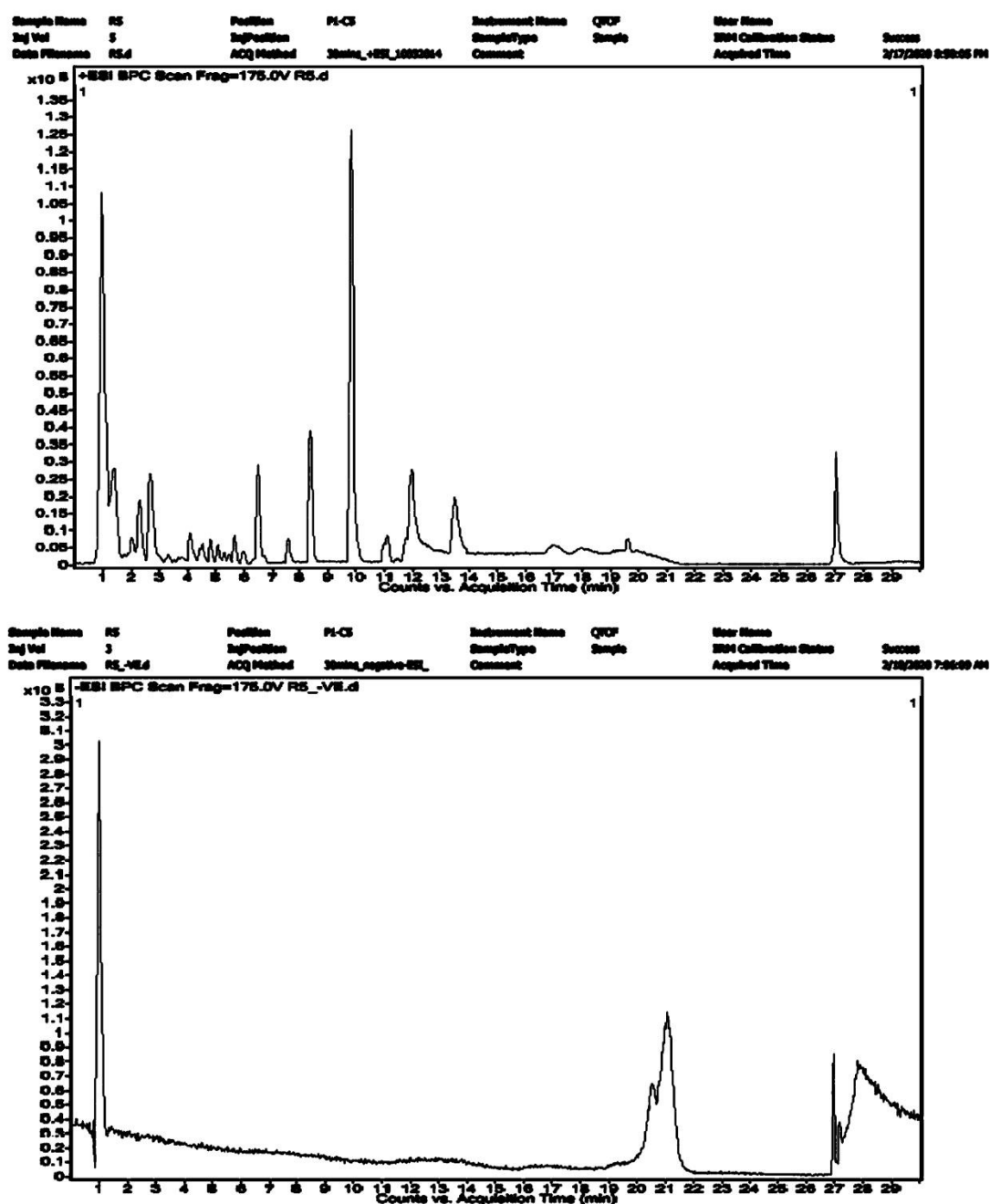


Fig. 4.5: HR-LC/MS analysis of crude extract of *G. saccatum* in +ve and -ve mode

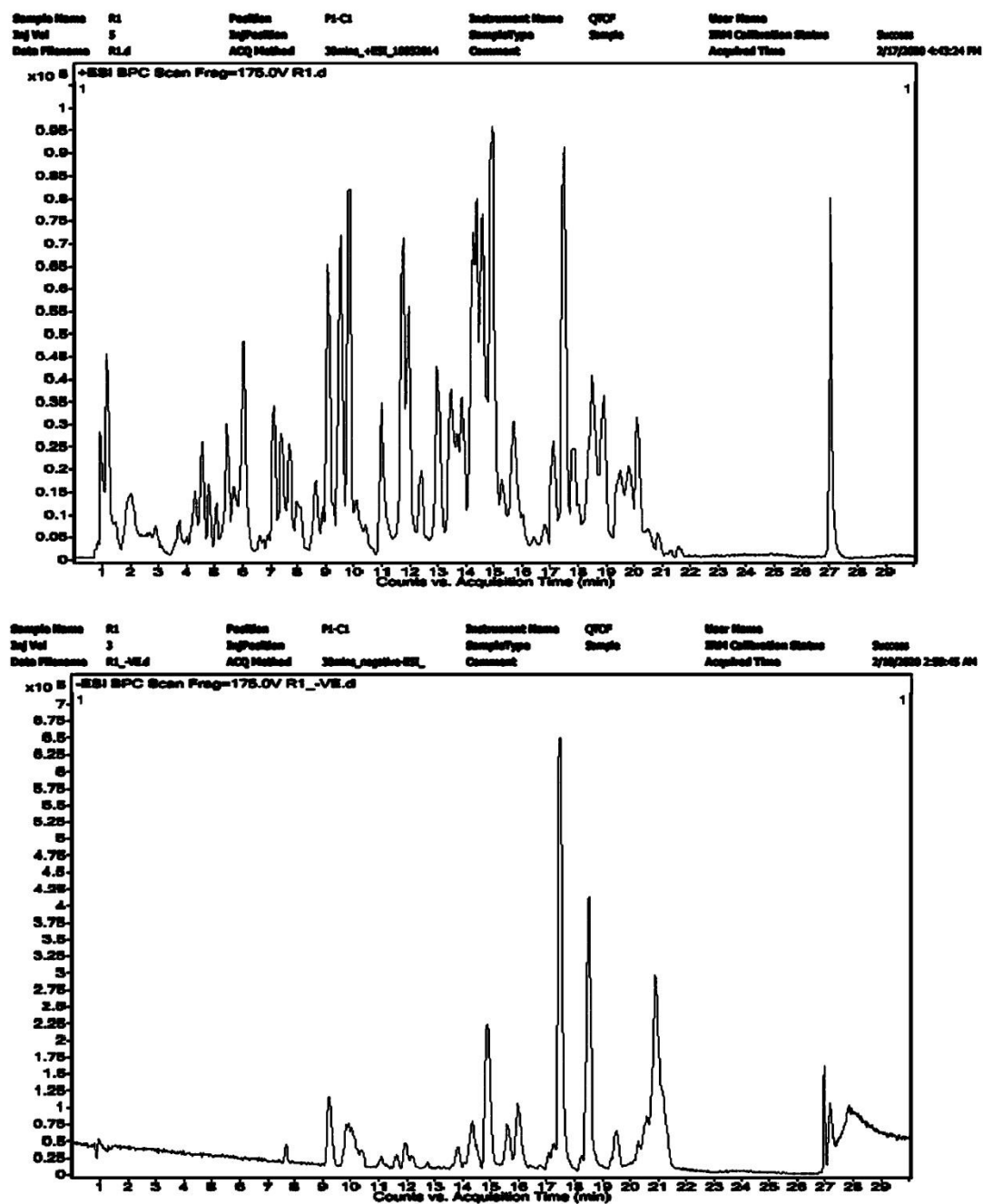


Fig. 4.6: HR-LC/MS analysis of crude extract of *D. indusiata* in +ve and -ve mode



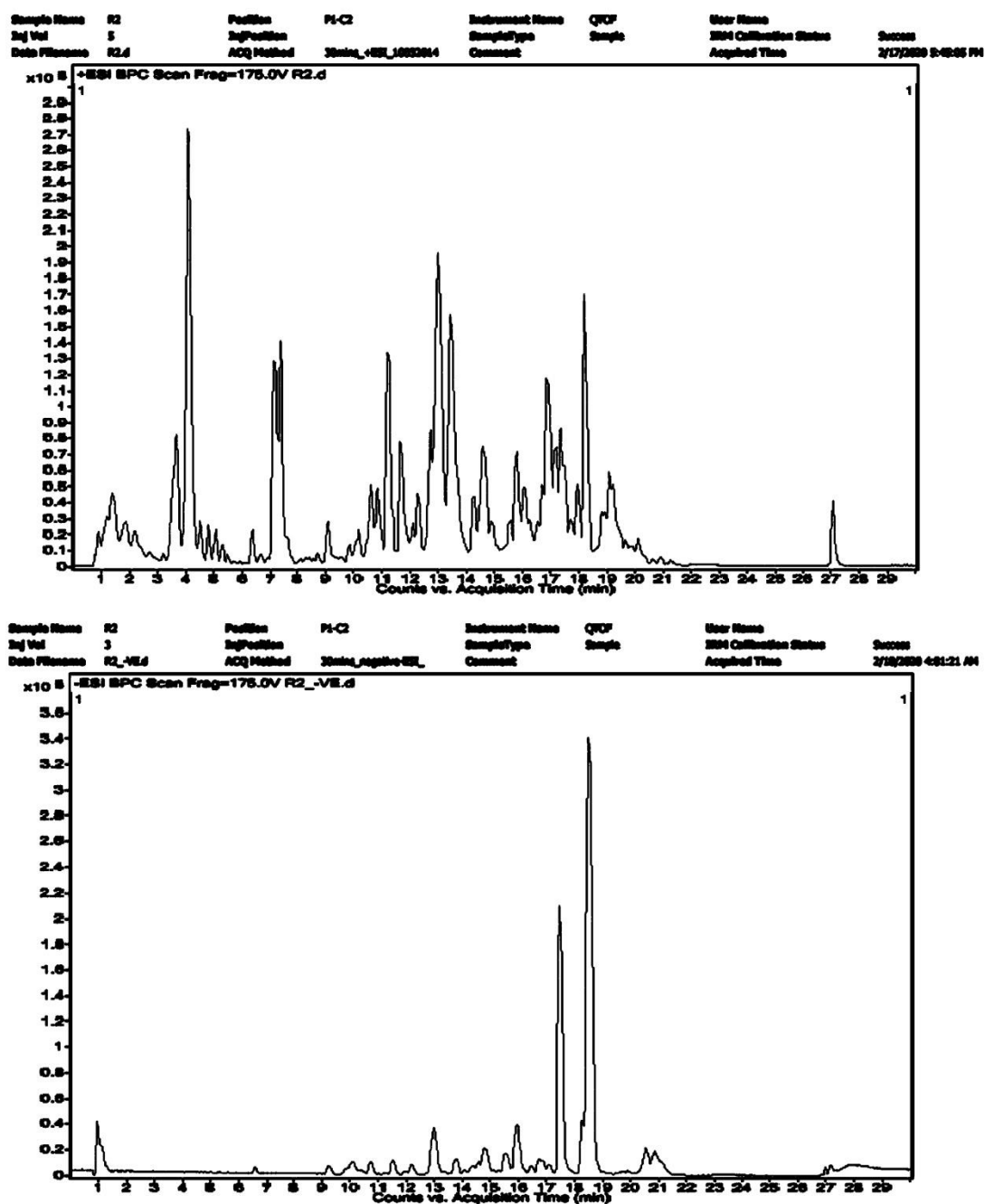


Fig. 4.7: HR-LC/MS analysis of crude extract of *I. galericulata* in +ve and -ve mode

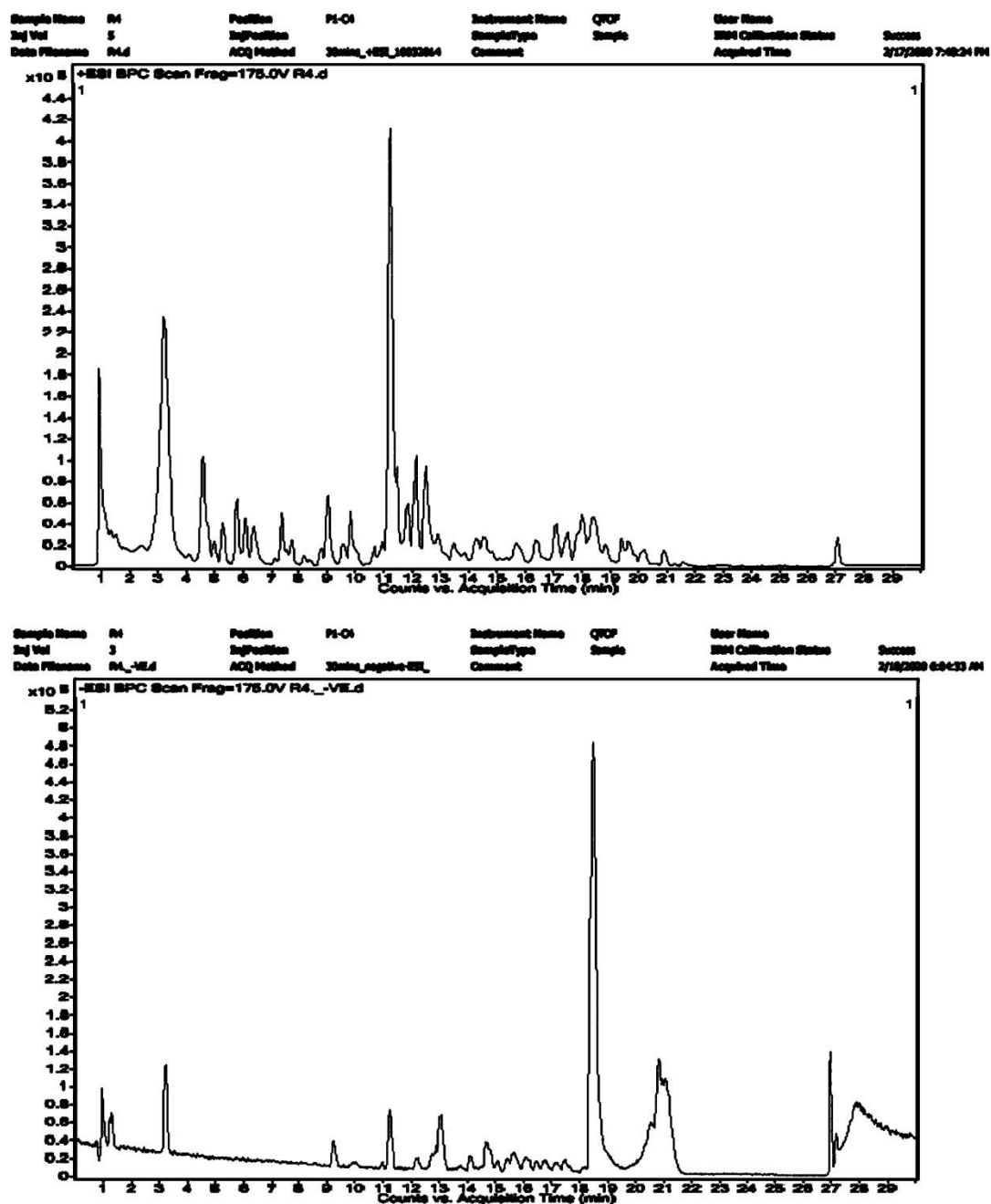


Fig. 4.8: HR-LC/MS analysis of crude extract of *C. stercoreus* in +ve and -ve mode

**Table 4.1:** Metabolite profiling of crude extract of *P. albus* with their therapeutic potential

Compound	<i>m/z</i>	Retention time	Mass	Formula	Therapeutic potential
L-Thyronine	272.0947	7.706	273.1022	C <sub>15</sub> H <sub>15</sub> NO <sub>4</sub>	Several formulations are used to treat hypothyroidism in the domestic animal (Feldman and Nelson, 1996)
Dodecyl glucoside	329.2357	9.216	348.2534	C <sub>18</sub> H <sub>36</sub> O <sub>6</sub>	-
Phloionolic acid	313.2413	12.022	332.2591	C <sub>18</sub> H <sub>36</sub> O <sub>5</sub>	-
9,13-dihydroxy-11-octadecenoic acid	295.2318	13.812	314.2497	C <sub>18</sub> H <sub>34</sub> O <sub>4</sub>	-
(6S)-1alpha,25-dihydroxyvitamin D3 6,19-sulfur dioxide adduct / (6S) 1alpha,25-Dihydroxycholecalciferol	479.2837	14.722	480.2901	C <sub>27</sub> H <sub>44</sub> O <sub>5</sub> S	-
1alpha,25-difluorovitamin D3 / 1alpha,25-Difluorocholecalciferol	455.2838	15.59	420.314	C <sub>27</sub> H <sub>42</sub> F <sub>2</sub> O	-
24,24-Difluoro-25-hydroxy-26,27 dimethyl vitamin D3	481.2996	15.917	464.3406	C <sub>29</sub> H <sub>46</sub> F <sub>2</sub> O <sub>2</sub>	-
9R-hydroxy-12E-octadecenoic acid	279.2381	17.459	298.256	C <sub>18</sub> H <sub>34</sub> O <sub>3</sub>	-
Docosanedioic acid	369.307	17.625	370.314	C <sub>22</sub> H <sub>42</sub> O <sub>4</sub>	-
DL-8-hydroxy stearic acid	299.2652	18.451	300.2724	C <sub>18</sub> H <sub>36</sub> O <sub>3</sub>	-
(23S)-1alpha,23,25-trihydroxy-24-	427.2928	19.397	446.3104	C <sub>27</sub> H <sub>42</sub> O <sub>5</sub>	-

oxovitamin D3 / (23S)-1alpha,23,25-trihydroxy-24-Oxocholecalciferol					
25-hydroxy-1alpha-hydroxymethyl-23,23,24,24-tetradhydrovitamin D3 / 25-hydroxy-1alpha-hydroxymethyl-23,23,24,24-tetradhydrocholecalciferol	407.3023	19.911	426.3199	C <sub>28</sub> H <sub>42</sub> O <sub>3</sub>	-
7-beta,12-alpha-Dihydroxy-3-oxo-5-beta-cholestan-26-oicacid	429.3079	20.319	448.326	C <sub>27</sub> H <sub>44</sub> O <sub>5</sub>	-
Practolol	265.1535	21.021	266.1604	C <sub>14</sub> H <sub>22</sub> N <sub>2</sub> O <sub>3</sub>	Utilized to treat of cardiac arrhythmias (PubChem)
Lupanine	265.1507	26.958	248.1918	C <sub>15</sub> H <sub>24</sub> N <sub>2</sub> O	Antidiabetic potential (Wiedemann et al., 2015)
Ropivacaine	309.1767	26.963	274.2064	C <sub>17</sub> H <sub>26</sub> N <sub>2</sub> O	Used in regional and obstetric anaesthesia during surgery (PubChem)

**Table 4.2:** Metabolite profiling of crude extract of *G. triplex* with their therapeutic potential

Compound	<i>m/z</i>	Retention time	Mass	Formula	Therapeutic potential
4-Amino-4-deoxychorismic acid	224.058	3.567	225.0651	C <sub>10</sub> H <sub>11</sub> NO <sub>5</sub>	-
Nitrazepam	316.0489	4.792	281.0797	C <sub>15</sub> H <sub>11</sub> N <sub>3</sub> O <sub>3</sub>	Used to treat insomnia (PubChem)
18-bromo-17E-octadecene	383.0451	9.081	348.0759	C <sub>18</sub> H <sub>21</sub> Br O <sub>2</sub>	-

Oxacillin	418.0617	9.67	401.103	C <sub>19</sub> H <sub>19</sub> N <sub>3</sub> O <sub>5</sub> S	Utilized to treat bacterial infections which is caused by gram-positive, susceptible organisms (PubChem)
Stictic acid	367.0505	10.668	386.0682	C <sub>19</sub> H <sub>14</sub> O <sub>9</sub>	Anticancer activity (Pejin et al., 2017)
Quercitrin	483.0771	11.639	448.106	C <sub>21</sub> H <sub>20</sub> O <sub>11</sub>	
<i>p</i> -Hydroxyphenobarbital glucuronide	459.0777	11.936	424.1086	C <sub>18</sub> H <sub>20</sub> N <sub>2</sub> O <sub>10</sub>	-
S-(4-Nitrobenzyl)glutathione	459.0775	12.343	442.1188	C <sub>17</sub> H <sub>22</sub> N <sub>4</sub> O <sub>8</sub> S	-

**Table 4.3:** Metabolite profiling of crude extract of *D. indusiata* with their therapeutic potential

Compound	<i>m/z</i>	Retention time	Mass	Formula	Therapeutic potential
Lactone	319.1477	0.838	296.1585	C <sub>16</sub> H <sub>24</sub> O <sub>5</sub>	Used to treat heart failure and high blood pressure (Drug Bank)
3-Hydroxymethyltriazolophthalazine none glucuronide	380.0925	0.88	375.113	C <sub>17</sub> H <sub>17</sub> N <sub>3</sub> O <sub>7</sub>	-
Mefenamic acid Metabolite (b-D-Glucopyranuronic acid, 1-[2-[(2,3-dimethylphenyl) amino] benzoate])	422.1242	0.922	417.1455	C <sub>21</sub> H <sub>23</sub> NO <sub>8</sub>	-

Sorbose	203.0511	0.928	180.0619	C <sub>6</sub> H <sub>12</sub> O <sub>6</sub>	-
Muramic acid	234.0953	0.971	251.0986	C <sub>9</sub> H <sub>17</sub> NO <sub>7</sub>	-
N-Acetyl-9-Olactoylneuraminic acid	382.1318	0.991	381.1246	C <sub>14</sub> H <sub>23</sub> NO <sub>11</sub>	-
Ketanserin	400.1423	0.995	395.1636	C <sub>22</sub> H <sub>22</sub> FN <sub>3</sub> O <sub>3</sub>	Antihypertensive medicine (PubChem)
Epimelibiose	365.1028	0.995	342.1136	C <sub>12</sub> H <sub>22</sub> O <sub>11</sub>	-
Cotarnine	260.0916	1.002	237.1023	C <sub>12</sub> H <sub>15</sub> NO <sub>4</sub>	-
Ketorolac	238.0899	1.004	255.0926	C <sub>15</sub> H <sub>13</sub> NO <sub>3</sub>	Non-steroidal anti-inflammatory drug (Drug Bank)
Glucosamine	184.0589	1.075	179.0803	C <sub>6</sub> H <sub>13</sub> NO <sub>5</sub>	-
Queuine	278.121	1.08	277.1138	C <sub>12</sub> H <sub>15</sub> N <sub>5</sub> O <sub>3</sub>	-
10-Hydroxydesmethylnortriptyline Glucuronide	442.1884	1.13	441.1802	C <sub>24</sub> H <sub>27</sub> NO <sub>7</sub>	-
2-Amino-4-hydroxy-6-(hydroxymethyl)-7,8-Dihydropteridine	200.0536	1.138	195.0751	C <sub>7</sub> H <sub>9</sub> N <sub>5</sub> O <sub>2</sub>	-
3',4'-dihydroxyflurbiprofen	259.0765	1.199	276.0798	C <sub>15</sub> H <sub>13</sub> FO <sub>4</sub>	-
3-Hydroxynorpromazine	309.1058	1.241	286.1161	C <sub>16</sub> H <sub>18</sub> N <sub>2</sub> OS	-

Kinetin	238.069	1.245	215.079	C <sub>10</sub> H <sub>9</sub> N <sub>5</sub> O	-
1,2-Benzenediol, 4-[[4-(4-fluorophenyl)-3-piperidinyl]methoxy]-, (3Strans)-	300.1417	1.25	317.1426	C <sub>18</sub> H <sub>20</sub> FNO <sub>3</sub>	-
Neuraminic acid	268.1033	1.257	267.0935	C <sub>9</sub> H <sub>17</sub> NO <sub>8</sub>	-
Modafinil	256.0797	1.263	273.0824	C <sub>15</sub> H <sub>15</sub> NO <sub>2</sub> S	Used in the treatment of narcolepsy (PubChem)
O-Succinyl-L-homoserine	220.0796	1.269	219.0724	C <sub>8</sub> H <sub>13</sub> NO <sub>6</sub>	-
N-Acetyl-9-Olactoylneuraminic Acid	382.1312	1.274	381.1243	C <sub>14</sub> H <sub>23</sub> NO <sub>11</sub>	-
Ketanserin	400.1422	1.289	395.1636	C <sub>22</sub> H <sub>22</sub> FN <sub>3</sub> O <sub>3</sub>	Used to treat chronic or acute vascular hypertension (PubChem)
Tiletamine	228.0848	1.3	223.1061	C <sub>12</sub> H <sub>17</sub> NOS	Anaesthetics, Dissociative, Anticonvulsants (PubChem)
2-Deoxysepiapterin	226.0691	1.347	221.0904	C <sub>9</sub> H <sub>11</sub> N <sub>5</sub> O <sub>2</sub>	-
3-Hydroxydesmethylnaprotiline Glucuronide	456.2047	1.369	455.1973	C <sub>25</sub> H <sub>29</sub> NO <sub>7</sub>	-

Nefopam	258.1314	1.447	253.1526	C <sub>17</sub> H <sub>19</sub> NO	Analgesics, Non-Narcotic (PubChem)
Propylthiouracilglucuronide	329.0819	1.452	346.0855	C <sub>13</sub> H <sub>18</sub> N <sub>2</sub> O <sub>7</sub> S	-
Prometon	230.1366	1.461	225.1581	C <sub>10</sub> H <sub>19</sub> N <sub>5</sub> O	-
Pantothenic Acid	224.0899	1.535	219.1105	C <sub>9</sub> H <sub>17</sub> NO <sub>5</sub>	-
Northiadene	304.1158	1.668	281.1261	C <sub>18</sub> H <sub>19</sub> NS	-
2-undecenal	173.1268	1.762	168.1481	C <sub>11</sub> H <sub>20</sub> O	-
3'-Desmethylpapaverine	308.132	1.852	325.1307	C <sub>19</sub> H <sub>19</sub> NO <sub>4</sub>	-
Bergenin	311.0712	2.061	328.0746	C <sub>14</sub> H <sub>16</sub> O <sub>9</sub>	
N-Carboxyethyl- gammaaminobutyric Acid	158.0798	2.307	175.083	C <sub>7</sub> H <sub>13</sub> NO <sub>4</sub>	-
L-2-Aminoadipic acid	166.0483	2.664	161.0698	C <sub>6</sub> H <sub>11</sub> N O <sub>4</sub>	-
Alaproclate	256.1159	3.765	255.1089	C <sub>13</sub> H <sub>18</sub> ClNO <sub>2</sub>	Anti-depressive agents (PubChem)
Tranexamic acid	180.0999	4.139	157.1108	C <sub>8</sub> H <sub>15</sub> NO <sub>2</sub>	Antifibrinolytic agents (PubChem)
Estradiol-17beta 3-sulfate	335.1305	4.194	352.1344	C <sub>18</sub> H <sub>24</sub> O <sub>5</sub> S	-
7-Desmethylprazosin	374.12	4.404	369.1417	C <sub>18</sub> H <sub>19</sub> N <sub>5</sub> O <sub>4</sub>	-



Quinine	325.1885	4.413	324.1821	C <sub>20</sub> H <sub>24</sub> N <sub>2</sub> O <sub>2</sub>	Antimalarials, Analgesics, Non-Narcotic, Muscle Relaxants (PubChem)
Netilmicin	476.303	5.03	475.2958	C <sub>21</sub> H <sub>41</sub> N <sub>5</sub> O <sub>7</sub>	Antibiotic (PubChem)
Carprofen	278.0321	5.423	273.0531	C <sub>15</sub> H <sub>12</sub> ClNO <sub>2</sub>	Non-steroidal anti-inflammatory drug (PubChem)
1alpha-hydroxy-23-[3-(1-hydroxy-1-methylethyl)phenyl]-22,22,23,23-tetradehydro-24,25,26,27-tetranorv	475.3225	5.649	474.3145	C <sub>32</sub> H <sub>42</sub> O <sub>3</sub>	-
(22S)-1alpha,22,25-trihydroxy-26,27-dimethyl-23,23,24,24-tetradehydro-24ahomovitamin D3 / (22S)-1al	453.3402	5.709	70.3436	C <sub>30</sub> H <sub>46</sub> O <sub>4</sub>	-
1-(8-[5]-ladderane-octanyl)-2-(8-[3]-ladderane-octanyl)-snlycerol	340.2575	6.558	634.5359	C <sub>43</sub> H <sub>70</sub> O <sub>3</sub>	-
10-nitro, 9Z, 12Z octadecadienoic acid	308.2197	7.593	325.2229	C <sub>18</sub> H <sub>31</sub> NO <sub>4</sub>	-
C16 Sphinganine	274.2725	9.809	273.2652	C <sub>16</sub> H <sub>35</sub> NO <sub>2</sub>	-
Phytosphingosine	318.2977	9.951	317.2904	C <sub>18</sub> H <sub>39</sub> NO <sub>3</sub>	-
Dihydrosphingosine	302.3034	11.118	301.296	C <sub>18</sub> H <sub>39</sub> NO <sub>2</sub>	-
Colforsin	415.2084	11.832	410.2297	C <sub>22</sub> H <sub>34</sub> O <sub>7</sub>	Anti-HIV agent, Adjuvants, Bronchodilator agents, Cardiotonic agents, Vasodilator agents (PubChem)

D-Pantetheine 4'-phosphate	341.091	14.124	358.0949	C <sub>11</sub> H <sub>23</sub> N <sub>2</sub> O <sub>7</sub> PS	-
3alpha,6beta,7alpha-Trihydroxy-5beta-cholan-24-oic acid	391.281	19.648	408.2846	C <sub>24</sub> H <sub>40</sub> O <sub>5</sub>	-
N-(2-hydroxyethyl) icosanamide	338.339	20.189	355.3422	C <sub>22</sub> H <sub>45</sub> NO <sub>2</sub>	-
Poloxalene	165.1119	27.022	164.1026	C <sub>7</sub> H <sub>16</sub> O <sub>4</sub>	-
Prometon	230.1381	27.089	225.1592	C <sub>10</sub> H <sub>19</sub> N <sub>5</sub> O	-
Methenamine	163.0965	27.09	140.1058	C <sub>6</sub> H <sub>12</sub> N <sub>4</sub>	Urinary tract antiseptic, antibiotic activity, ?Urinary anti-Infective agents (PubChem)
17-phenyl-trinor-PGF2alpha Amide	370.2428	27.12	387.2443	C <sub>23</sub> H <sub>33</sub> NO <sub>4</sub>	-

**Table 4.4:** Metabolite profiling of crude extract of *I. galariculata* with their therapeutic potential

Compound	<i>m/z</i>	Retention time	Mass	Formula	Therapeutic potential
Glucosamine	180.0864	0.994	179.0791	C <sub>6</sub> H <sub>13</sub> NO <sub>5</sub>	-
B-Octylglucoside	297.1648	1.059	292.186	C <sub>14</sub> H <sub>28</sub> O <sub>6</sub>	-
Citrulline	158.091	1.12	175.0945	C <sub>6</sub> H <sub>13</sub> N <sub>3</sub> O <sub>3</sub>	Used to treat dietary shortage or imbalance (PubChem)

Muramic acid	252.1071	1.476	251.0997	C <sub>9</sub> H <sub>17</sub> NO <sub>7</sub>	-
2-Amino-3-methoxy-benzoic acid	190.0482	6.354	167.0589	C <sub>8</sub> H <sub>9</sub> NO <sub>3</sub>	Used in the preparation of CDK1/cyclin B inhibitors for application towards antitumor treatment (Schultz et al., 1999)
10-nitro,9Z,12Zoctadecadienoic Acid	308.2199	7.276	325.2231	C <sub>18</sub> H <sub>31</sub> NO <sub>4</sub>	-
1,3-dipropyl-8-cyclopentylxanthine [DPCPX]	327.179	8.784	304.1898	C <sub>16</sub> H <sub>24</sub> N <sub>4</sub> O <sub>2</sub>	-
Tolterodine	348.2371	8.99	325.2478	C <sub>22</sub> H <sub>31</sub> NO	Used as anticholinergic agent to treat hyperactive bladder syndrome and urinary incontinence (PubChem)
Dihydrodeoxystreptomycin	568.2923	9.076	567.2852	C <sub>21</sub> H <sub>41</sub> N <sub>7</sub> O <sub>11</sub>	Antibiotic
N,N-(2,2-dihydroxy-ethyl) arachidonoyl amine	392.3128	9.95	391.3055	C <sub>24</sub> H <sub>41</sub> NO <sub>3</sub>	-
2-tetracosanamidoethanesulfonic acid	480.3499	10.9	475.3715	C <sub>26</sub> H <sub>53</sub> NO <sub>4</sub> S	-
Phytosphingosine	318.2982	11.166	317.2909	C <sub>18</sub> H <sub>39</sub> NO <sub>3</sub>	-
(±)13-Azaprostanoic acid	294.2767	11.457	311.28	C <sub>19</sub> H <sub>37</sub> NO <sub>2</sub>	Used as antagonist (Le Breton et al., 1979)
N-(16,16-dimethyl-5Z,8Z,11Z,14Zdocosatetraenoyl)-Ethanolamine	426.3333	11.716	403.3439	C <sub>26</sub> H <sub>45</sub> NO <sub>2</sub>	-
Colforsin	415.2082	11.834	410.2297	C <sub>22</sub> H <sub>34</sub> O <sub>7</sub>	Anti-HIV agent, Adjuvants, Bronchodilator agents, Cardiotonic agents, Vasodilator agents (PubChem)

N-(7Z,10Z,13Z,16Zdocosatetraenoyl)-ethanolamide	330.2799	11.851	347.2831	C <sub>22</sub> H <sub>37</sub> NO <sub>2</sub>	-
Dihydrosphingosine	302.3033	11.893	301.2942	C <sub>18</sub> H <sub>39</sub> NO <sub>2</sub>	-
Dihydroceramide C2	344.3131	12.137	343.3056	C <sub>20</sub> H <sub>41</sub> NO <sub>3</sub>	-
(Z)-N-(2-hydroxyethyl)icos-11-Enamide	358.3085	12.604	353.3298	C <sub>22</sub> H <sub>43</sub> NO <sub>2</sub>	-
N-(2-hydroxyethyl)icosanamide	360.3238	12.775	355.3451	C <sub>22</sub> H <sub>45</sub> NO <sub>2</sub>	-
Miltefosine	390.3188	12.942	407.3219	C <sub>21</sub> H <sub>46</sub> NO <sub>4</sub> P	Used in the treatment of both cutaneous and visceral leishmaniasis. It has a role as an antineoplastic agent, an antiprotozoal drug, an antifungal agent, an immunomodulator, an anti-inflammatory agent, an apoptosis inducer, a protein kinase inhibitor and an anti-coronaviral agent (PubChem)
Kanamycin	507.2242	13.263	484.2352	C <sub>18</sub> H <sub>36</sub> N <sub>4</sub> O <sub>11</sub>	As an antibiotic (PubChem)
11-hydroxy palmitic acid	277.2139	14.132	272.2352	C <sub>16</sub> H <sub>32</sub> O <sub>3</sub>	-
5S-hydroxy-hexadecanoic acid	295.2246	14.183	272.2356	C <sub>16</sub> H <sub>32</sub> O <sub>3</sub>	-
2-keto palmitic acid	275.1981	14.2	270.2195	C <sub>16</sub> H <sub>30</sub> O <sub>3</sub>	-
4,12-dihydroxy-hexadecanoic acid	293.2089	14.279	288.2302	C <sub>16</sub> H <sub>32</sub> O <sub>4</sub>	-
5,9-tetracosadienoic acid	369.3086	14.6	364.3299	C <sub>24</sub> H <sub>44</sub> O <sub>2</sub>	-
26,26,26-trifluoro-25-hydroxy-27-norvitamin D3 / 26,26,26-	423.2874	14.772	440.2899	C <sub>26</sub> H <sub>39</sub> F <sub>3</sub> O <sub>2</sub>	-

trifluoro-25-hydroxy-27-norcholecalciferol					
1alpha,2alpha,25-trihydroxy-19-norvitamin D3 / 1alpha,2alpha,25-trihydroxy-19-norcholecalciferolchol	425.3018	14.852	420.3242	C <sub>26</sub> H <sub>44</sub> O <sub>4</sub>	-
23-methyl-5Z,9Z-tetracosadienoic Acid	383.324	15.308	378.3454	C <sub>25</sub> H <sub>46</sub> O <sub>2</sub>	-
27-nor-5b-cholestane-3a,7a,12a,24,25-pentol	443.3126	15.7	438.3342	C <sub>26</sub> H <sub>46</sub> O <sub>5</sub>	-
2-Nor-1,3-seco-1alpha,25-dihydroxyvitamin D3	427.3176	15.704	404.3284	C <sub>26</sub> H <sub>44</sub> O <sub>3</sub>	-
9,14,19,19,19-pentadeuterio-1alpha,25-dihydroxyprevitamin D3 / 9,14,19,19,19-pentadeuterio-1alpha,25	444.3442	16.379	421.3549	C <sub>27</sub> H <sub>39</sub> D <sub>5</sub> O <sub>3</sub>	-
Methoprene (S)	315.2292	17.149	310.2506	C <sub>19</sub> H <sub>34</sub> O <sub>3</sub>	-
(17E)-1alpha,25-dihydroxy-17,20-didehydro-21-norvitamin D3 / (17E)-1alpha,25-dihydroxy-17,20-Didehyd	405.2753	17.186	400.2967	C <sub>26</sub> H <sub>40</sub> O <sub>3</sub>	-
N-(2-hydroxyethyl)palmitamide	282.2771	17.384	299.2804	C <sub>18</sub> H <sub>37</sub> NO <sub>2</sub>	-
Dicyclomine	314.2456	17.593	309.2669	C <sub>19</sub> H <sub>35</sub> NO <sub>2</sub>	Anticholinergic agent used to treat gastrointestinal conditions (PubChem)

25-dihydroxy-19-nor-3-epivitamin D3 / 25-dihydroxy-19-nor-3-epicholecalciferol	411.3226	18.36	388.3333	C <sub>26</sub> H <sub>44</sub> O <sub>2</sub>	-
o-Hydroxyfinasteride	389.2806	19.382	388.2735	C <sub>23</sub> H <sub>36</sub> N <sub>2</sub> O <sub>3</sub>	-
DL-PDMP	391.2934	19.654	390.2863	C <sub>23</sub> H <sub>38</sub> N <sub>2</sub> O <sub>3</sub>	-
Prometon	230.1383	27.133	225.1589	C <sub>10</sub> H <sub>19</sub> N <sub>5</sub> O	-

**Table 4.5:** Metabolite profiling of crude extract of *C. stereoreus* with their therapeutic potential

Compound	m/z	Retention time	Mass	Formula	Therapeutic potential
3,5-Pyridinedicarboxylic acid, 1,4-dihydro-2,6-dimethyl-4-(2-nitrophenyl)-, 2-hydroxy-2-methylpropyl	387.1182	0.93	406.136	C <sub>19</sub> H <sub>22</sub> N <sub>2</sub> O <sub>8</sub>	-
Nitrendipine	377.0897	1.047	360.1308	C <sub>18</sub> H <sub>20</sub> N <sub>2</sub> O <sub>6</sub>	Used as a calcium-channel blocker to treat hypertension (PubChem)
Etanidazole	195.0534	1.075	214.0713	C <sub>7</sub> H <sub>10</sub> N <sub>4</sub> O <sub>4</sub>	A nitroimidazole drug that was investigated in clinical trials for its radio sensitizing properties in cancer treatment (Drug Bank)
Sulfinpyrazone	439.0894	1.146	404.1203	C <sub>23</sub> H <sub>20</sub> N <sub>2</sub> O <sub>3</sub> S	Uricosuric drug (PubChem)
Dodecyl glucoside	329.2375	10.152	348.2553	C <sub>18</sub> H <sub>36</sub> O <sub>6</sub>	-

Phloionolic acid	331.2533	11.483	332.2606	C <sub>18</sub> H <sub>36</sub> O <sub>5</sub>	-
8,9-dihydroxy stearic acid	315.2586	13.014	316.2658	C <sub>18</sub> H <sub>36</sub> O <sub>4</sub>	-
N-(2R-methyl-3-hydroxy-ethyl)- 16,16-dimethyl-5Z,8Z,11Z,14Z- docosatetraenoylamine	416.3433	14.517	417.3506	C <sub>27</sub> H <sub>47</sub> NO <sub>2</sub>	-
19'-Hexanoyloxyfucoxanthinol	747.4389	15.538	730.4798	C <sub>46</sub> H <sub>66</sub> O <sub>7</sub>	-
PGE2alpha dimethyl amine	366.3073	16.866	367.3145	C <sub>22</sub> H <sub>41</sub> NO <sub>3</sub>	-
9R-hydroxy-12E-octadecenoic Acid	279.2389	17.627	298.2569	C <sub>18</sub> H <sub>34</sub> O <sub>3</sub>	-
1-hexadecanoyl-sn-glycerol	311.2654	18.179	330.2831	C <sub>19</sub> H <sub>38</sub> O <sub>4</sub>	-
DL-8-hydroxy stearic acid	299.2657	18.439	300.2729	C <sub>18</sub> H <sub>36</sub> O <sub>3</sub>	-
1-(9Z-hexadecenoyl)-2- (9Zheptadecenoyl)-sn-glycerol	279.239	18.689	578.5026	C <sub>36</sub> H <sub>66</sub> O <sub>5</sub>	-
Practolol	265.1533	20.368	266.1602	C <sub>14</sub> H <sub>22</sub> N <sub>2</sub> O <sub>3</sub>	Used to treat cardiac arrhythmias (PubChem)
2-hydroxy-nonadecanoic acid		20.397	314.2788	C <sub>19</sub> H <sub>38</sub> O <sub>3</sub>	-
Dipalmitoylphosphatidic acid	349.2482	20.572	648.4796	C <sub>35</sub> H <sub>69</sub> O <sub>8</sub> P	-
Dihydroartemisinin	265.1502	26.945	284.1679	C <sub>15</sub> H <sub>24</sub> O <sub>5</sub>	

#### ***4.3.5. In silico analysis of fungal metabolites as potential inhibitors against main protease of SARS-CoV-2***

Based on medicinal uses and binding energy, active sites were covered after molecular docking analysis; three potent compounds (bergenin, quercitrin and dihydroartemisinin) were selected for in-depth *in-silico* analysis as potential inhibitors against SARS-CoV-2 M<sup>pro</sup>.

##### ***4.3.5.1. Virtual screening***

The crystal structure of SARS-CoV-2 M<sup>pro</sup> in complex with inhibitor N3 to 2.1-Å resolution was determined by Jin et al. (2020). The SARS-CoV-2 M<sup>pro</sup> has a Cys-His catalytic dyad. Each protomer of SARS-CoV-2 M<sup>pro</sup> is composed of three domains (**Fig. 4.9C**). Domains I and Domains II have an antiparallel  $\beta$ -barrel structure which are extended from residues 8-101 and residues 102-184, respectively. Domain III ranges from residues 201-303 and contains five  $\alpha$ -helices arranged into antiparallel globular cluster. Domain II and Domain III are connected by a long loop region extended from residues 185-200. The substrate-binding site is situated in a cleft between Domain I and II. The inhibitor, N3 binds in the substrate-binding pocket. The backbone of N3 forms an antiparallel sheet with 164 to 168 residues (His164, Met165, Glu166, Leu167, Pro168) of the long strand 155-168 on one side. The backbone of N3 also forms an antiparallel sheet with residues 189-191 (Gln189, Thr190, Ala191) of the loop linking domains II and III. The inhibitor N3 makes van der Waals bond, conventional hydrogen bond, carbon-hydrogen bond, amide  $\pi$ -stacked interaction, alkyl and  $\pi$ -alkyl interactions with different residues of SARS-CoV-2 M<sup>pro</sup> (**Fig. 4.9D**) (Jin et al., 2020). The binding energy of inhibitor N3 as predicted by AutoDock 4.2 was -6.2 kcal/mol (**Table 4.7**).



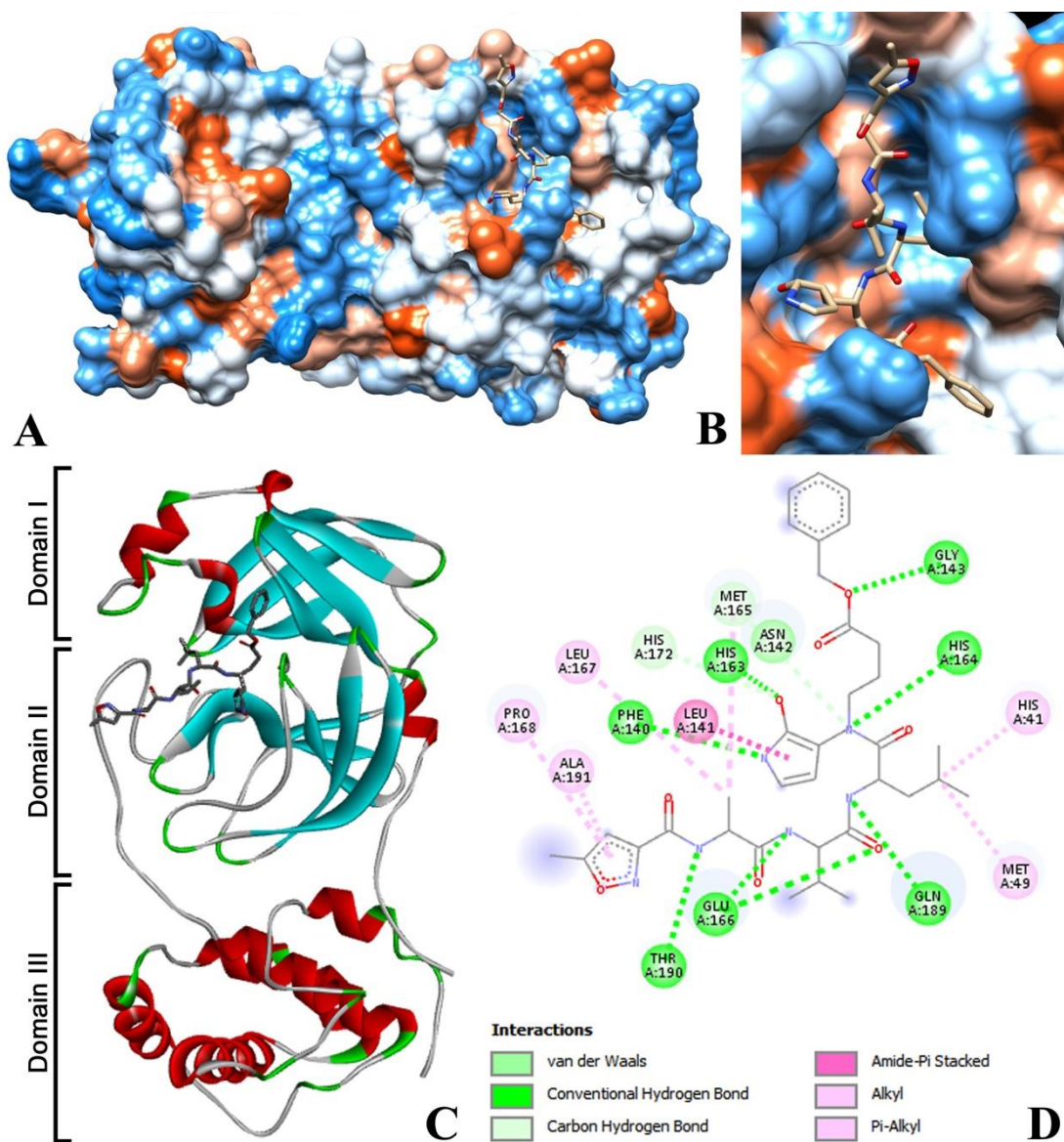


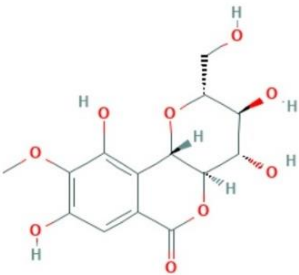
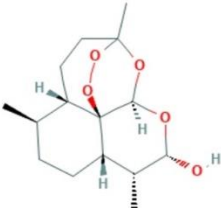
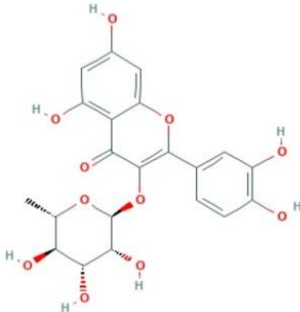
**Fig. 4.9:** Interaction of N3 in the binding cleft of SARS-CoV-2 M<sup>pro</sup> (A) hydrophobicity surface 3D representation (B) Interaction of N3 in a pocket site of SARS-CoV-2 M<sup>pro</sup> (C) the crystal structure of SARS-CoV-2 M<sup>pro</sup> in complex with an inhibitor N3 (D) 2D representation describing all possible bindings in active site of SARS-CoV-2 M<sup>pro</sup>

The compounds that did not acquire more than 2 violations of Lipinski's rule were selected for molecular docking. The results of bioactive compound scanning using Lipinski's rule of five are shown in **Table 4.6**. These features are important for the

identification of molecular drug ability. The detailed results of the binding energies and ZINC identification of each selected ligand are shown in **Table 4.7**. Lower binding energy values as well as maximum interactions with active site residues within the target M<sup>pro</sup> of 6LU7 were evaluated for selecting the best pharmacophore-like drug-candidates. The lowest binding energies achieved from docking 6LU7 M<sup>pro</sup> with the ligands bergenin, dihydroartemisinin and quercitrin were -7.93, -7.23 and -10.36 kcal/mol, respectively. The mean binding energies achieved from docking 6LU7 M<sup>pro</sup> with the ligands bergenin, dihydroartemisinin and quercitrin were -7.86, -7.20 and -10.29 kcal/mol, respectively (**Table 4.7**). The binding affinity seemed higher as compared to inhibitor N3 (-6.2 kcal/mol). The type and amount of bonding are essential for the high affinity of compounds with the active site of the protein. Bergenin forms many chemical bonds with seven active residues PHE140, GLY143, CYS145, HIS163, HIS164, GLU166 and GLN189 of 6LU7 M<sup>pro</sup> receptor (**Fig. 4.10D**). Dihydroartemisinin forms many chemical bonds with only three active residues GLY143, CYS145 and HIS163 of 6LU7 M<sup>pro</sup> receptor (**Fig. 4.12D**). Many chemical bonds were observed with only four active residues CYS145, HIS163, GLU166 and THR190 of 6LU7 M<sup>pro</sup> receptor in the case of quercitrin. However, several amino acids other than active residues were also bonded with the 6LU7 M<sup>pro</sup> receptor. Hence, binding affinity seems higher for quercitrin as compared to bergenin and dihydroartemisinin (**Fig. 4.11D**). These findings ranked the inhibition potential of tested compounds as per binding energy in the following order: quercitrin>bergenin>dihydroartemisinin. However, considering the number of active sites bonded, the rank of the inhibition potential of tested compounds is bergenin>quercitrin>dihydroartemisinin.

The docking analysis of bergenin (**Fig. 4.10**) indicated that active residue HIS163 exhibited conventional H-bond,  $\pi$ -cation electrostatic interaction and  $\pi$ -hydrophobic and  $\pi$ - $\pi$ -T shaped hydrophobic interactions with bergenin. Active residue GLN189 showed conventional H-bond, carbon-hydrogen bond and  $\pi$ -donor hydrogen bond interactions with bergenin. Conventional hydrogen bond interactions were also observed with an active residue of GLY143 and GLU166. Carbon-hydrogen bond and  $\pi$ -donor hydrogen bond interactions were found with PHE140 and HIS164 (**Fig. 4.13A**). Active residue CYS145 formed  $\pi$ -alkyl hydrophobic interactions with bergenin (**Fig. 4.13B**). Additionally, two more interactions, conventional H-bond and carbon-hydrogen interaction, were observed with SER144 and HIS41, respectively.

**Table 4.6:** Properties of SARS-CoV-2 M<sup>pro</sup> potential inhibitors

No	Compound	Structure	Source	Molecular formula	Lipinski's rule of five	
					Properties	Value
1	Bergenin		<i>Dictyophora indusiata</i>	C <sub>14</sub> H <sub>16</sub> O <sub>9</sub>	Molecular weight (<500 g/mol)	328.27 g/mol
					LogP (<5)	-1.201
					H-Bond donor (<5)	5
					H-bond acceptor (<10)	9
					Violations	0
2	Dihydroartemisinin		<i>Cyathus stercoreus</i>	C <sub>15</sub> H <sub>24</sub> O <sub>5</sub>	Molecular weight (<500 g/mol)	284.35 g/mol
					LogP (<5)	2.5
					H-Bond donor (<5)	1
					H-bond acceptor (<10)	5
					Violations	0
3	Quercitrin		<i>Gaeastrum triplex</i>	C <sub>21</sub> H <sub>20</sub> O <sub>11</sub>	Molecular weight (<500 g/mol)	448.38 g/mol
					LogP (<5)	0.9
					H-Bond donor (<5)	7
					H-bond acceptor (<10)	11
					Violations	2

**Table 4.7:** Molecular docking analysis of potential compounds against SARS-CoV-2 M<sup>pro</sup>

No.	Compound	Zinc/Pubchem ID	Lowest Binding	Mean Binding
			Energy	Energy
			(kcal/mol)	(kcal/mol)
1	Bergenin	ZINC4046820	-7.93	-7.86
2	Dihydroartemisinin	Pubchem CID_456410	-7.23	-7.20
3	Quercitrin	ZINC4175638	-10.36	-10.29
4	N3- Peptide-like		-6.6	-6.2

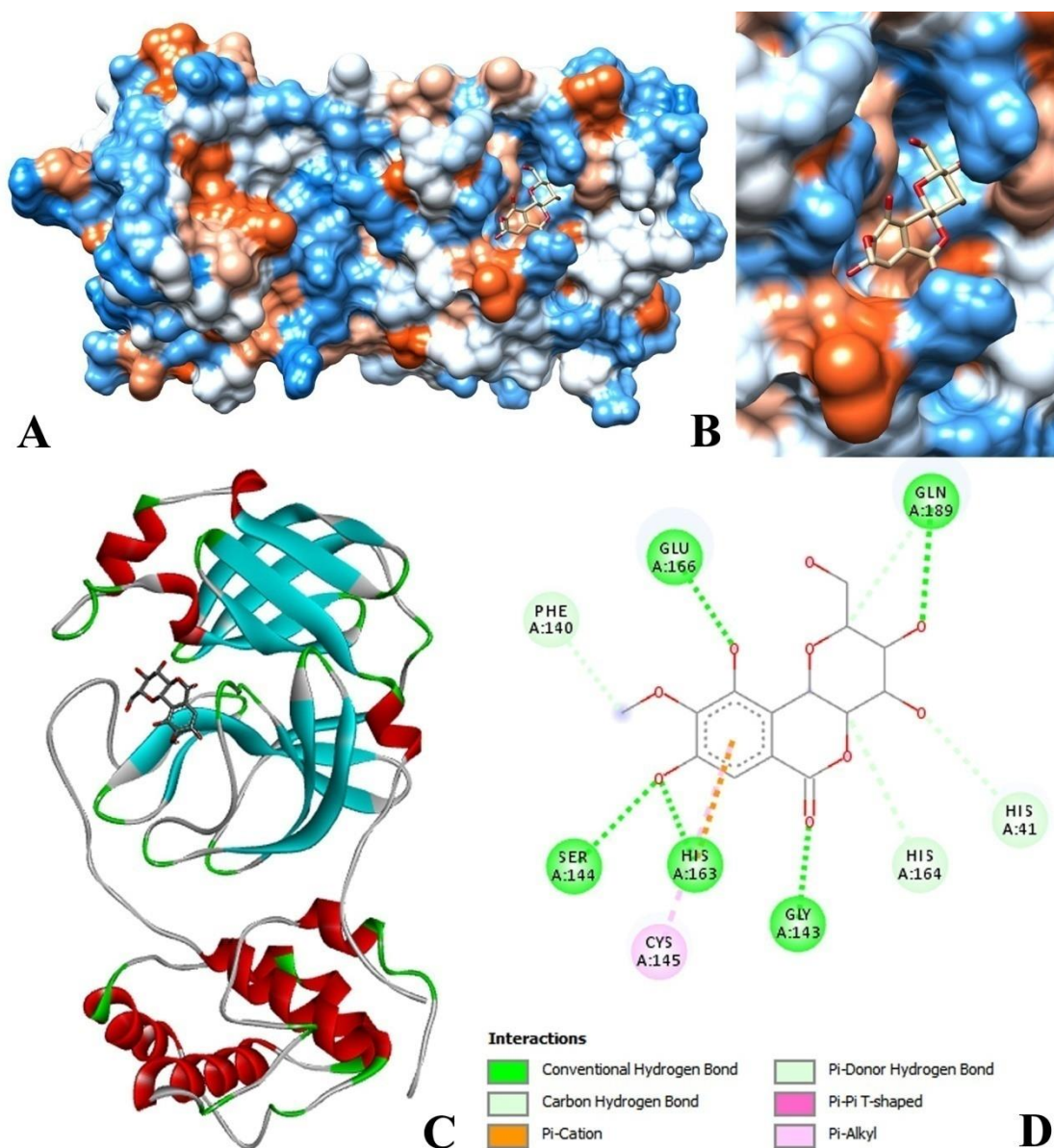


**Fig. 4.10:** Docking analysis visualization of SARS-CoV-2 M<sup>pro</sup> binding with Bergenin (A) hydrophobicity surface 3D representation (B) Interaction of Bergenin in a pocket site of SARS-CoV-2 M<sup>pro</sup> (C) 3D representation of Bergenin-SARS-CoV-2 M<sup>pro</sup> interaction (D) 2D representation describing bindings of Bergenin in active site of SARS-CoV-2 M<sup>pro</sup>



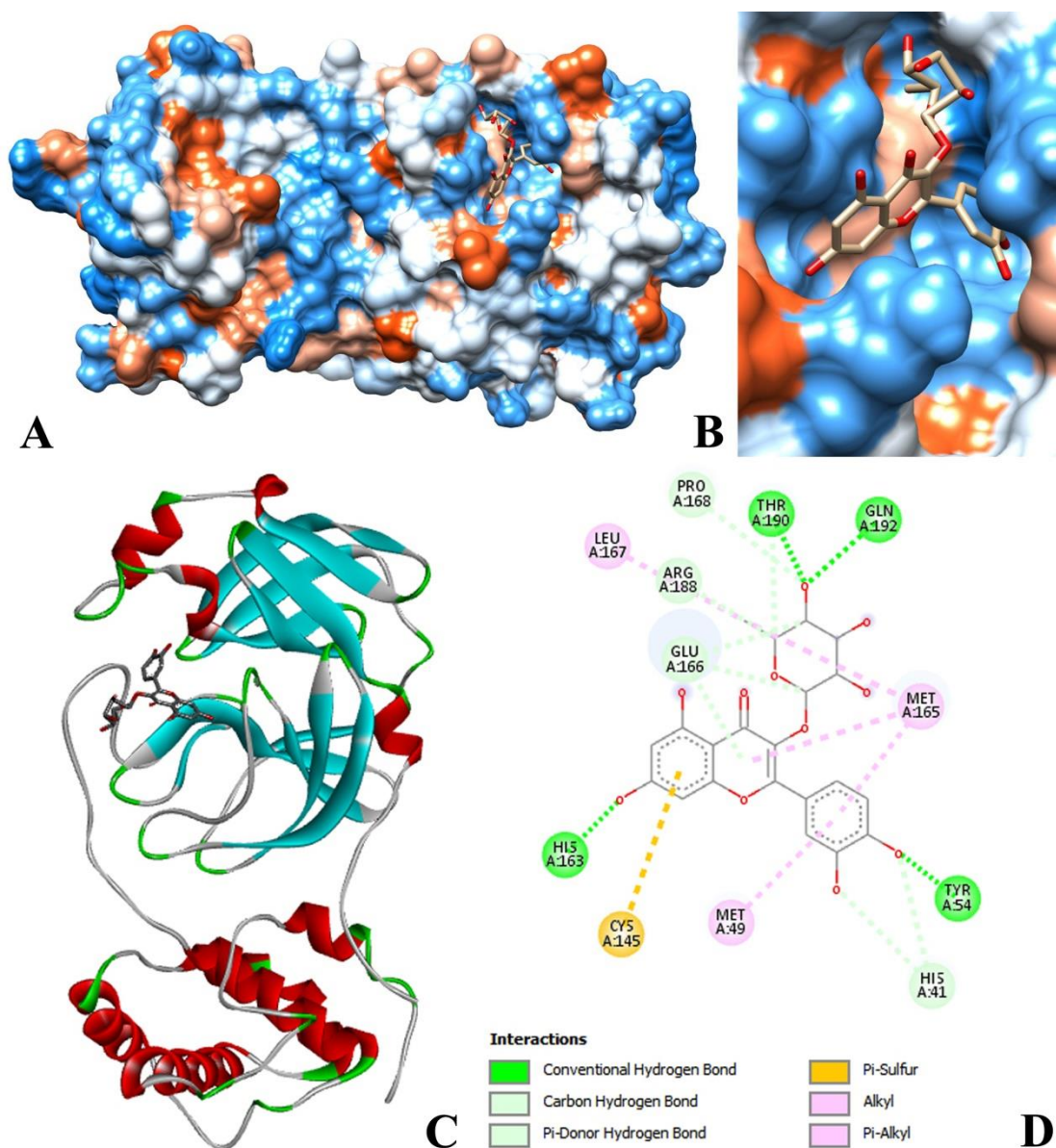


**Fig. 4.11:** Docking analysis visualization of SARS-CoV-2 M<sup>pro</sup> binding with Quercitrin (A) hydrophobicity surface 3D representation (B) Interaction of Quercitrin in a pocket site of SARS-CoV-2 M<sup>pro</sup> (C) 3D representation of Quercitrin-SARS-CoV-2 M<sup>pro</sup> interaction (D) 2D representation describing bindings of Quercitrin in active site of SARS-CoV-2 M<sup>pro</sup>

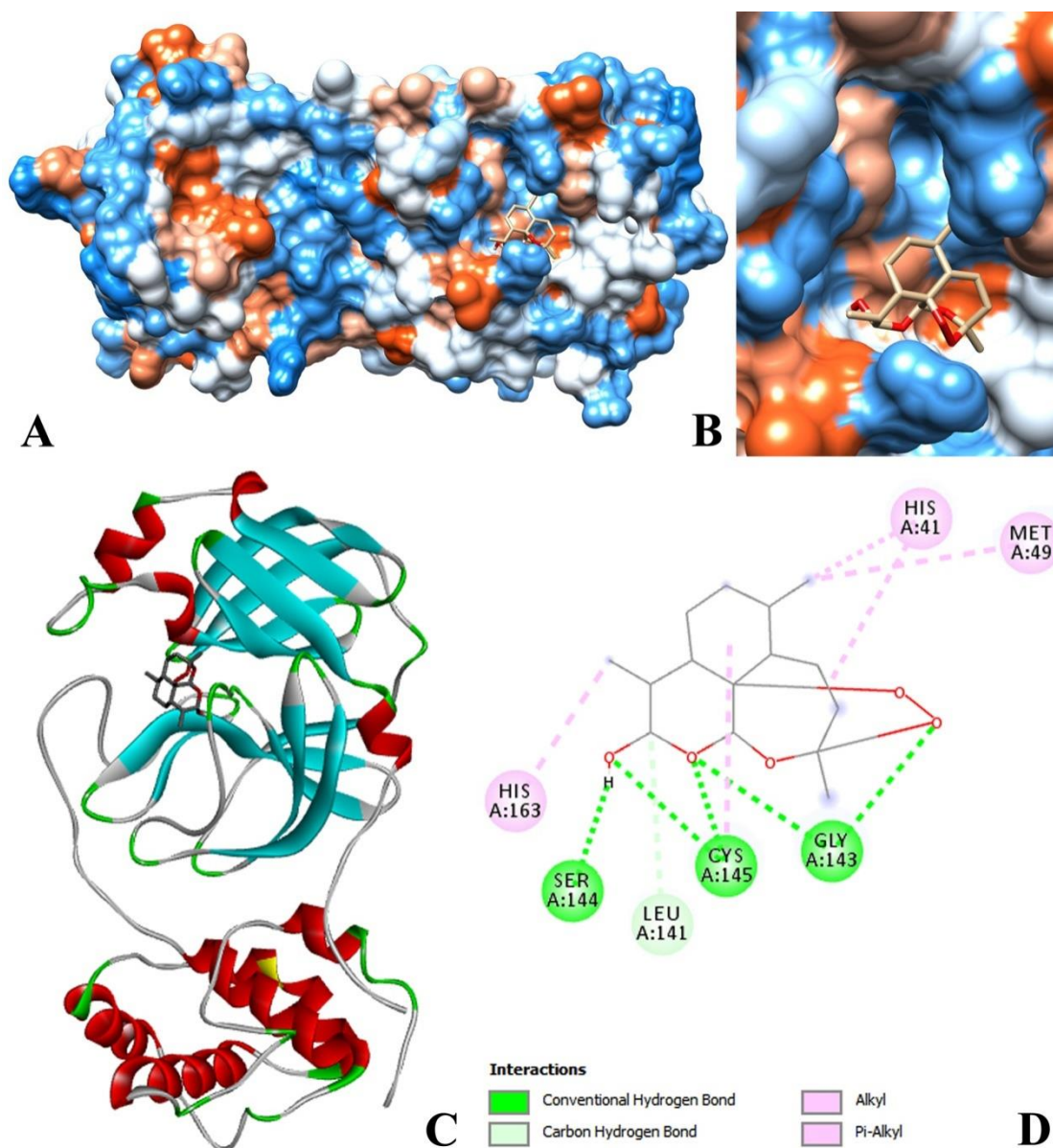


**Fig. 4.12:** Docking analysis visualization of SARS-CoV-2 M<sup>pro</sup> binding with Dihydroartemisinin (A) hydrophobicity surface 3D representation (B) Interaction of Dihydroartemisinin in a pocket site of SARS-CoV-2 M<sup>pro</sup> (C) 3D representation of Dihydroartemisinin-SARS-CoV-2 M<sup>pro</sup> interaction (D) 2D representation describing bindings of Dihydroartemisinin in active site of SARS-CoV-2 M<sup>pro</sup>



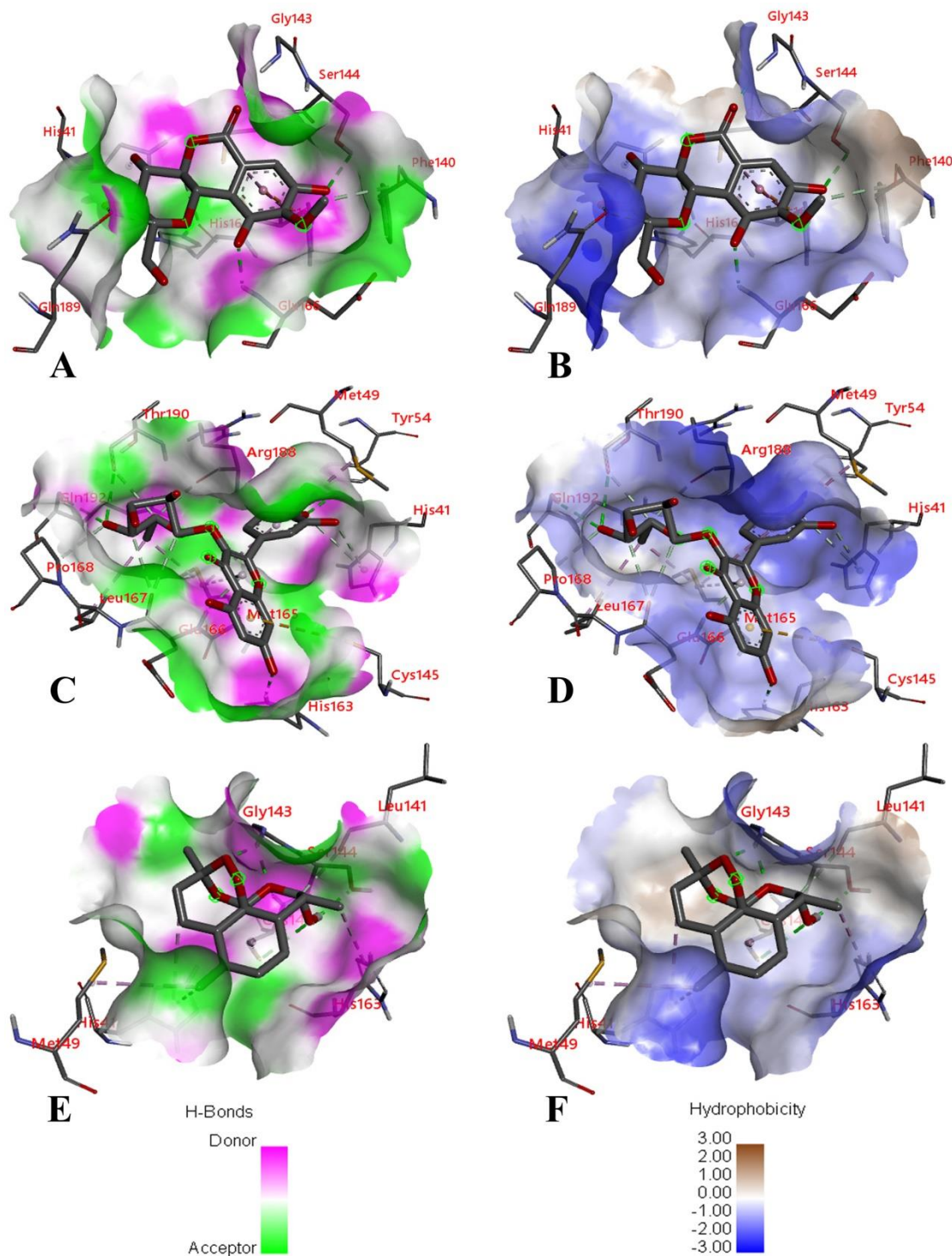


**Fig. 4.13:** Interactions of compounds with H-bond and hydrophobic in a pocket site of SARS-CoV-2 M<sup>pro</sup> (A), (C) and (E) show H-bond interaction of Bergenin, Quercitrin and Dihydroartemisinin; (B), (D) and (F) show hydrophobic interaction of Bergenin, Quercitrin and Dihydroartemisinin

The docking analysis of bergenin (**Fig. 4.10**) indicated that active residue HIS163 exhibited conventional H-bond,  $\pi$ -cation electrostatic interaction and  $\pi$ -hydrophobic and  $\pi$ - $\pi$ -T shaped hydrophobic interactions with bergenin. Active residue GLN189 showed conventional H-bond, carbon-hydrogen bond and  $\pi$ -donor hydrogen bond interactions with bergenin. Conventional hydrogen bond interactions were also observed with an active residue of GLY143 and GLU166. Carbon-hydrogen bond and  $\pi$ -donor hydrogen bond interactions were found with PHE140 and HIS164 (**Fig. 4.13A**). Active residue CYS145 formed  $\pi$ -alkyl hydrophobic interactions with bergenin (**Fig. 4.13B**). Additionally, two more interactions, conventional H-bond and carbon-hydrogen interaction, were observed with SER144 and HIS41, respectively.

The docking analysis of quercitrin is shown in **Fig. 4.11**. The results indicated that conventional H-bond was observed with active residue HIS163, THR190 and with other amino acids TYR54 and GLN192. The active residue GLU166, THR190 and other amino acids PRO168, ARG188, HIS41 exhibited both carbon-hydrogen bond and  $\pi$ -donor hydrogen bond interactions with quercitrin (**Fig. 4.13C**). Amino acids LEU 167 and MET165 formed alkyl hydrophobic interactions, whereas amino acids MET165 and MET49 formed  $\pi$ -alkyl hydrophobic interactions with quercitrin (**Fig. 4.13D**). Additionally, active residue CYS145 interacted by a sulphur bond with quercitrin.

The results of the docking analysis of dihydroartemisinin are shown in **Fig. 4.12**. The results indicated that active residue CYS145 exhibited conventional H-bond and alkyl hydrophobic interactions with dihydroartemisinin (**Fig. 4.13E** and **4.13F**). Conventional H-bond and  $\pi$ -alkyl hydrophobic interactions were found with the active residues GLY143 and HIS163, respectively. Amino acid SER144, LEU141, MET49

and HIS41 exhibited conventional H-bond, carbon-hydrogen bond, alkyl hydrophobic interactions and  $\pi$ -alkyl hydrophobic interactions with dihydroartemisinin, respectively.

#### 4.3.5.2. ADMET study

ADMET predictions of the bergenin, quercitrin and dihydroartemisinin were carried out using the pkCSM pharmacokinetics server, which is shown in **Table 4.8**. Based on VDss data, bergenin showed better distribution (0.946 log L/kg) followed by dihydroartemisinin (0.503 log L/kg) and quercitrin (-0.262 log L/kg). The results of fraction unbound also showed the more effective abilities of these three compounds for distribution in tissues of the body. All the three compounds did not interfere in the cytochrome (CYP) metabolism and had better renal clearance. The renal clearance was found much better in dihydroartemisinin followed by quercitrin and bergenin. Moreover, hepatotoxicity and skin sensitisation were also not predicted by all the three compounds. The results of the ADMET study further specified the drug ability potential of bergenin, quercitrin and dihydroartemisinin.

Bergenin, dihydroartemisinin and quercitrin have been reported for various medicinal uses previously (Piacente et al., 1996; Zuo et al., 2005; Singh et al., 2009; Rajbhandari et al., 2011; Patel et al., 2012; Bajracharya, 2015; Sheahan et al., 2020). Bergenin is a C-glucoside of 4-O-methyl gallic acid and has long been used as folk medicine in many parts of Asia (Patel et al., 2012). It is poorly soluble in water and is easily degraded in a basic solution (Bajracharya, 2015). The molecular formula and chemical structure are shown in **Table 4.6**. Bergenin exhibits antiparasitic, antihepatotoxic, antiviral, anti-HIV, antiarrhythmic, antiulcerogenic, neuroprotective, immunomodulatory, antioxidant, antimicrobial and anti-inflammatory properties

(Singh et al., 2009). Anti-HIV activity of bergenin was reported with an effective concentration ( $EC_{50}$ ) of 40  $\mu\text{g/mL}$  (Piacente et al., 1996). Bergenin also displayed antiviral activity against Hepatitis C virus with an  $IC_{50}$  of 1.71 mM (Zuo et al., 2005). Antiviral activity of bergenin was also reported against herpes simplex virus type-1 with an  $IC_{50}$  value of  $<6.25 \mu\text{g/mL}$  (Rajbhandari et al., 2011). Additionally, Bergenin was also reported for good antiparasitic activity with an  $IC_{50}$  value of 2.4  $\mu\text{g/mL}$  against *Plasmodium falciparum*, a chloroquine-sensitive strain (Uddin et al., 2013).

Quercitrin is a glycoside made from the quercetin flavonoid and the deoxy sugar rhamnose. It was reported to show antiviral activity against dengue virus infection with an  $IC_{50}$  value of 467.27  $\mu\text{g/mL}$  (Chiow et al., 2016). Quercitrin displayed inhibition against HIV-1 reverse transcriptase (Yu et al., 2007) and antiviral activity against hepatitis C virus (HCV) (Aoki et al., 2014). Quercitrin also showed proliferation inhibition of *Plasmodium falciparum* with an  $IC_{50}$  value of 1.1  $\mu\text{g/mL}$  (Liu et al., 2007). It also exhibited antimicrobial, antidiarrhoeic, antileishmanial and anti-inflammatory properties (Galvez et al., 1993; Comalada et al., 2005; Muzitano et al., 2006; Hasan et al., 2014;). Above findings indicate that bergenin and quercitrin could be used against SARS-CoV-2 as these have been shown to possess good antiviral activity against hepatitis and HIV viruses similar to remdesivir as well as antiparasitic activity similar to chloroquine, drugs which are being used currently for the treatment of SARSCoV-2 (Sheahan et al., 2020).

**Table 4.8:** ADMET prediction of the bergenin, quercitrin and dihydroartemisinin

	Bergenin	Quercitrin	Dihydroartemisinin
<b>Absorption</b>			
Water solubility (log mol/L)	-2.068	-3.006	-3.124
CaCO <sub>2</sub> permeability (log Papp in 10 <sup>-6</sup> cm/s)	0.363	-0.576	1.228
Intestinal absorption (% Absorbed)	34.88	50.59	95.071
Skin Permeability (log Kp)	-2.735	-2.735	-3.764
P-glycoprotein substrate	Yes	Yes	No
P-glycoprotein I inhibitor	No	No	No
P-glycoprotein II inhibitor	No	No	No
<b>Distribution</b>			
VDss (human) (log L/kg)	0.946	-0.262	0.503
Fraction unbound (human) (Fu)	0.562	0.182	0.438
BBB permeability (log BB)	-1.334	-1.683	0.393
CNS permeability (log PS)	-4.267	-4.708	-2.901
<b>Metabolism</b>			
CYP2D6 substrate	No	No	No
CYP3A4 substrate	No	No	No
CYP1A2 inhibitor	No	No	No
CYP2C19 inhibitor	No	No	No
CYP2C9 inhibitor	No	No	No
CYP2D6 inhibitor	No	No	No
CYP3A4 inhibitor	No	No	No
<b>Excretion</b>			
Total Clearance (log ml/min/kg)	0.5	0.624	0.99
Renal OCT2 substrate	No	No	No
<b>Toxicity</b>			
AMES toxicity	No	No	No
Max. tolerated dose (human) (log mg/kg/day)	-0.122	0.426	-0.371
hERG I inhibitor	No	No	No
hERG II inhibitor	No	Yes	No
Oral Rat Acute Toxicity (LD50) (mol/kg)	2.387	2.662	2.781
Oral Rat Chronic Toxicity (LOAEL) (log mg/kg_bw/day)	3.868	3.762	1.925
Hepatotoxicity	No	No	No
Skin Sensitisation	No	No	No
<i>Tetrahymenapyriformis</i> toxicity (µg/L)	0.285	0.285	0.306
Minnow toxicity (mM)	4.207	1.828	1.73

Dihydroartemisinin, an artemisinin derivative, is more water-soluble and is a safe and most effective antimalarial drug. Dihydroartemisinin is generally used with a combination of piperazine, a popular regimen recommended by WHO against

malaria (Keating, 2012). The dihydroartemisinin was reported to show 50% inhibition ( $IC_{50}$ ) of *Plasmodium falciparum* growth in vitro in the low nanomolar range (Keating, 2012). As shown in (Fig. 4.12), dihydroartemisinin binds with the pocket region of active sites of 6LU7 Mpro; therefore, it may be a probable potential molecule against SARS-CoV-2. Further studies are needed to confirm the potential of this drug.

The docking analysis, ADMET predictions and medicinal properties clearly indicate that bergenin, quercitrin and dihydroartemisinin are the most significant compounds as potential inhibitors of SARS-CoV-2 M<sup>pro</sup>, which could be explored further.

#### 4.4. References

- Andrade, B., Ghosh, P., Barth, D., Tiwari, S., Santana, R.J., Silva, W.R. de A.S., Melo, T.S., dos Santos Freitas, A., González-Grande, P., Palmeira, L.S., 2020. Computational screening for potential drug candidates against SARS-CoV-2 main protease.
- Aoki, C., Hartati, S.R.I., Santi, M.R., Firdaus, R., Hanafi, M., Kardono, L.B.S., Shimizu, Y., Sudarmono, P.P., Hotta, H., 2014. Isolation and identification of substances with anti-hepatitis C virus activities from *Kalanchoe pinnata*. Int. J. Pharm. Pharm. Sci. 6, 211-215.
- Bajracharya, G.B., 2015. Diversity, pharmacology and synthesis of bergenin and its derivatives: potential materials for therapeutic usages. Fitoterapia 101, 133-152.
- Blois, M.S., 1958. Antioxidant determinations by the use of a stable free radical. Nature 181, 1199-1200.
- Bray, F., Ferlay, J., Soerjomataram, I., Siegel, R.L., Torre, L.A., Jemal, A., 2018. Global cancer statistics 2018: GLOBOCAN estimates of incidence and mortality worldwide for 36 cancers in 185 countries. CA. Cancer J. Clin. 68, 394-424.
- Chio, K.H., Phoon, M.C., Putti, T., Tan, B.K.H., Chow, V.T., 2016. Evaluation of antiviral activities of *Houttuynia cordata* Thunb. extract, quercetin, quercitrin and cinanserin on murine coronavirus and dengue virus infection. Asian Pac. J. Trop. Med. 9, 1-7.



- Comalada, M., Camuesco, D., Sierra, S., Ballester, I., Xaus, J., Gálvez, J., Zarzuelo, A., 2005. In vivo quercitrin anti-inflammatory effect involves release of quercetin, which inhibits inflammation through down-regulation of the NF- $\kappa$ B pathway. *Eur. J. Immunol.* 35, 584-592.
- Drug Bank. <https://go.drugbank.com/drugs/>. Accessed on 28 April, 2020.
- Evidente, A., Kornienko, A., Cimmino, A., Andolfi, A., Lefranc, F., Mathieu, V., Kiss, R., 2014. Fungal metabolites with anticancer activity. *Nat. Prod. Rep.* 31, 617-627.
- Feldman, E.C., Nelson, R.W., 1996. Canine and feline endocrinology and reproduction, 2nd ed. WB Saunders, Philadelphia.
- Galvez, J., Crespo, M.E., Jimenez, J., Suarez, A., Zarzuelo, A., 1993. Antidiarrhoeic activity of quercitrin in mice and rats. *J. Pharm. Pharmacol.* 45, 157-159.
- Hasan, S., Singh, K., Danisuddin, M., Verma, P.K., Khan, A.U., 2014. Inhibition of major virulence pathways of *Streptococcus* mutans by quercitrin and deoxynojirimycin: a synergistic approach of infection control. *PLoS One* 9.
- Hyde, K.D., Xu, J., Rapior, S., Jeewon, R., Lumyong, S., Niego, A.G.T., Abeywickrama, P.D., Aluthmuhandiram, J.V.S., Brahmananage, R.S., Brooks, S., 2019. The amazing potential of fungi: 50 ways we can exploit fungi industrially. *Fungal Divers.* 97, 1-136.
- Iqbal, J., Abbasi, B.A., Mahmood, T., Kanwal, S., Ali, B., Shah, S.A., Khalil, A.T., 2017. Plant-derived anticancer agents: A green anticancer approach. *Asian Pac. J. Trop. Biomed.* 7, 1129-1150.
- Jin, Z., Du, X., Xu, Y., Deng, Y., Liu, M., Zhao, Y., Zhang, B., Li, X., Zhang, L., Peng, C., 2020. Structure of Mpro from SARS-CoV-2 virus and discovery of its inhibitors. *Nature* 582, 289-293.
- Keating, G.M., 2012. Dihydroartemisinin/Piperaquine. *Drugs* 72, 937-961.
- Khaerunnisa, S., Kurniawan, H., Awaluddin, R., Suhartati, S., Soetjipto, S., 2020. Potential inhibitor of COVID-19 main protease ( $M^{pro}$ ) from several medicinal plant compounds by molecular docking study. Prepr. doi10.20944/preprints202003.0226.v1 1-14.
- Le Breton, G.C., Venton, D.L., Enke, S.E., Halushka, P. V, 1979. 13-Azaprostanoic acid: a specific antagonist of the human blood platelet thromboxane/endoperoxide receptor. *Proc. Natl. Acad. Sci.* 76, 4097-4101.

- Lipinski, C.A., Lombardo, F., Dominy, B.W., Feeney, P.J., 1997. Experimental and computational approaches to estimate solubility and permeability in drug discovery and development settings. *Adv. Drug Deliv. Rev.* 23, 3-25.
- Liu, X., Chen, Y., Wu, L., Wu, X., Huang, Y., Liu, B., 2017. Optimization of polysaccharides extraction from *Dictyophora indusiata* and determination of its antioxidant activity. *Int. J. Biol. Macromol.* 103, 175-181.
- Liu, Y., Murakami, N., Ji, H., Abreu, P., Zhang, S., 2007. Antimalarial Flavonol Glycosides from *Euphorbia hirta*. *Pharm. Biol.* 45, 278-281.
- Martín, J.-F., García-Estrada, C., Zeilinger, S., 2014. Biosynthesis and molecular genetics of fungal secondary metabolites. Springer.
- Mau, J.-L., Lin, H.-C., Song, S.-F., 2002. Antioxidant properties of several specialty mushrooms. *Food Res. Int.* 35, 519-526.
- Morris, G.M., Huey, R., Lindstrom, W., Sanner, M.F., Belew, R.K., Goodsell, D.S., Olson, A.J., 2009. AutoDock4 and AutoDockTools4: Automated docking with selective receptor flexibility. *J. Comput. Chem.* 30, 2785-2791.
- Muzitano, M.F., Tinoco, L.W., Guette, C., Kaiser, C.R., Rossi-Bergmann, B., Costa, S.S., 2006. The antileishmanial activity assessment of unusual flavonoids from *Kalanchoe pinnata*. *Phytochemistry* 67, 2071-2077.
- O Oyetayo, V., Dong, C.-H., Yao, Y.-J., 2009. Antioxidant and antimicrobial properties of aqueous extract from *Dictyophora indusiata*. *Open Mycol. J.* 3.
- Patel, D.K., Patel, K., Kumar, R., Gadewar, M., Tahilyani, V., 2012. Pharmacological and analytical aspects of bergenin: a concise report. *Asian Pacific J. Trop. Dis.* 2, 163-167.
- Pejin, B., Iodice, C., Bogdanović, G., Kojić, V., Tešević, V., 2017. Stictic acid inhibits cell growth of human colon adenocarcinoma HT-29 cells. *Arab. J. Chem.* 10, S1240-S1242.
- Piacente, S., Pizza, C., De Tommasi, N., Mahmood, N., 1996. Constituents of *Ardisia japonica* and their in vitro anti-HIV activity. *J. Nat. Prod.* 59, 565-569.
- Pires, D.E. V, Blundell, T.L., Ascher, D.B., 2015. pkCSM: predicting small-molecule pharmacokinetic and toxicity properties using graph-based signatures. *J. Med. Chem.* 58, 4066-4072.
- PubChem. <https://pubchem.ncbi.nlm.nih.gov/>. Accessed on 28 April, 2020.
- Rajbhandari, M., Lalk, M., Mentel, R., Lindequist, U., 2011. Antiviral Activity and



- Constituents of the Nepalese Medicinal Plant *Astilbe rivularis*. Rec. Nat. Prod. 5.
- Rathee, S., Rathee, Dharmender, Rathee, Deepti, Kumar, V., Rathee, P., 2012. Mushrooms as therapeutic agents. Rev. Bras. Farmacogn. 22, 459-474.
- Schrödinger, 2020. The PyMOL Molecular Graphics System, Version 2.3.
- Schultz, C., Link, A., Leost, M., Zaharevitz, D.W., Gussio, R., Sausville, E.A., Meijer, L., Kunick, C., 1999. Paullones, a series of cyclin-dependent kinase inhibitors: synthesis, evaluation of CDK1/cyclin B inhibition, and in vitro antitumor activity. J. Med. Chem. 42, 2909-2919.
- Seetharaman, P., Gnanasekar, S., Chandrasekaran, R., Chandrakasan, G., Kadarkarai, M., Sivaperumal, S., 2017. Isolation and characterization of anticancer flavone chrysin (5, 7-dihydroxy flavone)-producing endophytic fungi from *Passiflora incarnata* L. leaves. Ann. Microbiol. 67, 321-331.
- Sheahan, T.P., Sims, A.C., Leist, S.R., Schäfer, A., Won, J., Brown, A.J., Montgomery, S.A., Hogg, A., Babusis, D., Clarke, M.O., 2020. Comparative therapeutic efficacy of remdesivir and combination lopinavir, ritonavir, and interferon beta against MERS-CoV. Nat. Commun. 11, 1-14.
- Singh, U., Barik, A., Priyadarsini, K.I., 2009. Reactions of hydroxyl radical with bergenin, a natural poly phenol studied by pulse radiolysis. Bioorg. Med. Chem. 17, 6008-6014.
- Smedsgaard, J., Nielsen, J., 2005. Metabolite profiling of fungi and yeast: from phenotype to metabolome by MS and informatics. J. Exp. Bot. 56, 273-286.
- Sung, H., Ferlay, J., Siegel, R.L., Laversanne, M., Soerjomataram, I., Jemal, A., Bray, F., 2021. Global cancer statistics 2020: GLOBOCAN estimates of incidence and mortality worldwide for 36 cancers in 185 countries. CA. Cancer J. Clin. 71, 209-249.
- SWISSADME. <http://www.swissadme.ch/>. Accessed on 28 April, 2020.
- Uddin, G., Sadat, A., Siddiqui, B.S., 2013. Comparative antioxidant and antiplasmodial activities of 11-O-galloylbergenin and bergenin isolated from *Bergenia ligulata*. World Appl. Sci. J. 27, 977-981.
- Wang, M., Cao, R., Zhang, L., Yang, X., Liu, J., Xu, M., Shi, Z., Hu, Z., Zhong, W., Xiao, G., 2020. Remdesivir and chloroquine effectively inhibit the recently emerged novel coronavirus (2019-nCoV) in vitro. Cell Res. 30, 269-271.
- Wiedemann, M., Gurrola-Díaz, C.M., Vargas-Guerrero, B., Wink, M., García-López,

- P.M., Düfer, M., 2015. Lupanine improves glucose homeostasis by influencing KATP channels and insulin gene expression. *Molecules* 20, 19085-19100.
- Yu, Y.-B., Miyashiro, H., Nakamura, N., Hattori, M., Park, J.C., 2007. Effects of triterpenoids and flavonoids isolated from *Alnus firma* on HIV-1 viral enzymes. *Arch. Pharm. Res.* 30, 820.
- Zhang, L., Lin, D., Sun, X., Curth, U., Drosten, C., Sauerhering, L., Becker, S., Rox, K., Hilgenfeld, R., 2020. Crystal structure of SARS-CoV-2 main protease provides a basis for design of improved  $\alpha$ -ketoamide inhibitors. *Science*. 368, 409–412.
- Zhang, Q.-Y., Wang, F.-X., Jia, K.-K., Kong, L.-D., 2018. Natural product interventions for chemotherapy and radiotherapy-induced side effects. *Front. Pharmacol.* 1253.
- Zhao, G.-R., Xiang, Z.-J., Ye, T.-X., Yuan, Y.-J., Guo, Z.-X., 2006. Antioxidant activities of *Salvia miltiorrhiza* and *Panax notoginseng*. *Food Chem.* 99, 767-774.
- ZINC database <https://zinc15.docking.org/>. Accessed on 28 April, 2020.
- Zuo, G.-Y., Li, Z.-Q., Chen, L.-R., Xu, X.-J., 2005. In vitro anti-HCV activities of *Saxifraga melanocentra* and its related polyphenolic compounds. *Antivir. Chem. Chemother.* 16, 393-398.